ACS Infectious Diseases

Article

pubs.acs.org/journal/aidcbc

Essential but Not Vulnerable: Indazole Sulfonamides Targeting Inosine Monophosphate Dehydrogenase as Potential Leads against *Mycobacterium tuberculosis*

Yumi Park,[†] Angela Pacitto,[‡] Tracy Bayliss,[§] Laura A. T. Cleghorn,[§] Zhe Wang,[⊗] Travis Hartman,[⊗] Kriti Arora,[†] Thomas R. Ioerger,[⊥] Jim Sacchettini,[#] Menico Rizzi,[Γ] Stefano Donini,[Γ] Tom L. Blundell,[‡] David B. Ascher,[‡] Kyu Rhee,[⊗] Ardala Breda,[#] Nian Zhou,[#] Veronique Dartois,[Δ] Surendranadha Reddy Jonnala,[†] Laura E. Via,[†,Θ] Valerie Mizrahi,[Θ] Ola Epemolu,[§] Laste Stojanovski,[§] Fred Simeons,[§] Maria Osuna-Cabello,[§] Lucy Ellis,[§] Claire J. MacKenzie,[§] Alasdair R. C. Smith,[§] Susan H. Davis,[§] Dinakaran Murugesan,[§] Kirsteen I. Buchanan,[§] Penelope A. Turner,[§] Margaret Huggett,[§] Fabio Zuccotto,[§] Maria Jose Rebollo-Lopez,[Ξ] Maria Jose Lafuente-Monasterio,[Ξ] Olalla Sanz,[Ξ] Gracia Santos Diaz,[Ξ] Joël Lelièvre,[Ξ] Lluis Ballell,[Ξ] Carolyn Selenski,[Σ] Matthew Axtman,[Σ] Sonja Ghidelli-Disse,[Φ] Hannah Pflaumer,[Φ] Markus Bösche,[Φ] Gerard Drewes,[Φ] Gail M. Freiberg,[Ω] Matthew D. Kurnick,[Ω] Myron Srikumaran,[Ω] Dale J. Kempf,[Ω] Simon R. Green,[§] Peter C. Ray,[§] Kevin Read,[§] Paul Wyatt,[§] Clifton E. Barry, III,[†,Θ] and Helena I. Boshoff*[,†]

[†]Tuberculosis Research Section, Laboratory of Clinical Infectious Diseases, National Institute of Allergy and Infectious Disease, National Institutes of Health, Bethesda, Maryland 20892-3206, United States

[‡]Department of Biochemistry, University of Cambridge, Cambridge CB2 1GA, United Kingdom

[§]Drug Discovery Unit, College of Life Sciences, James Black Centre, University of Dundee, Dundee DD1 5EH, United Kingdom

[⊗]Division of Infectious Diseases, Department of Medicine, Weill Cornell Medical College, New York, New York 10065, United States

[⊥]Department of Computer Science and Engineering, Texas A&M University, College Station, Texas 77843, United States

[#]Department of Biochemistry & Biophysics, Texas A&M University, College Station, Texas 77843, United States

[Γ]Dipartimento di Scienze del Farmaco, University of Piemonte Orientale, Via Bovio 6, 28100 Novara, Italy

[Δ]Public Health Research Institute, New Jersey Medical School, Rutgers, The State University of New Jersey, Newark, New Jersey 07103, United States

[Θ]MRC/NHLS/UCT Molecular Mycobacteriology Research Unit, Institute of Infectious Disease and Molecular Medicine, University of Cape Town, Rondebosch 7700, South Africa

[Ξ]Diseases of the Developing World, GlaxoSmithKline, Calle Severo Ochoa 2, 28760 Tres Cantos, Madrid, Spain

[Σ]GlaxoSmithKline, 5 Crescent Drive, Philadelphia, Pennsylvania 19112, United States

[Φ]Cellzome GmbH, Molecular Discovery Research, GlaxoSmithKline, Meyerhofstrasse 1, 69117 Heidelberg, Germany

[Ω]AbbVie Molecular Characterization, 1 North Waukegan Road, North Chicago, Illinois 60064, United States

Supporting Information

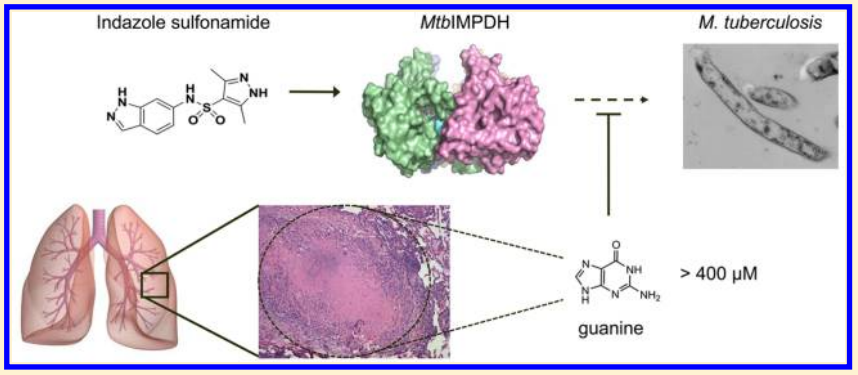

ABSTRACT: A potent, noncytotoxic indazole sulfonamide was identified by high-throughput screening of >100,000 synthetic compounds for activity against *Mycobacterium tuberculosis* (*Mtb*). This noncytotoxic compound did not directly inhibit cell wall

continued...

Received: June 12, 2016
Published: October 5, 2016

DOI: 10.1021/acsinfecdis.6b00103
ACS Infect. Dis. 2017, 3, 18−33

biogenesis but triggered a slow lysis of *Mtb* cells as measured by release of intracellular green fluorescent protein (GFP). Isolation of resistant mutants followed by whole-genome sequencing showed an unusual gene amplification of a 40 gene region spanning from *Rv3371* to *Rv3411c* and in one case a potential promoter mutation upstream of *guaB2* (*Rv3411c*) encoding inosine monophosphate dehydrogenase (IMPDH). Subsequent biochemical validation confirmed direct inhibition of IMPDH by an uncompetitive mode of inhibition, and growth inhibition could be rescued by supplementation with guanine, a bypass mechanism for the IMPDH pathway. Beads containing immobilized indazole sulfonamides specifically interacted with IMPDH in cell lysates. X-ray crystallography of the IMPDH−IMP−inhibitor complex revealed that the primary interactions of these compounds with IMPDH were direct pi−pi interactions with the IMP substrate. Advanced lead compounds in this series with acceptable pharmacokinetic properties failed to show efficacy in acute or chronic murine models of tuberculosis (TB). Time−kill experiments in vitro suggest that sustained exposure to drug concentrations above the minimum inhibitory concentration (MIC) for 24 h were required for a cidal effect, levels that have been difficult to achieve in vivo. Direct measurement of guanine levels in resected lung tissue from tuberculosis-infected animals and patients revealed 0.5−2 mM concentrations in caseum and normal lung tissue. The high lesional levels of guanine and the slow lytic, growth-rate-dependent effect of IMPDH inhibition pose challenges to developing drugs against this target for use in treating TB.

KEYWORDS: *target validation, IMPDH, guanine, purine salvage, Mycobacterium tuberculosis, indazole sulfonamide*

As the incidence of drug-resistant tuberculosis (TB) continues to worsen, there is a pressing need for new agents to treat this recalcitrant disease.[1] One of the key drivers of drug resistance is the lengthy 6-month course of therapy that must be completed to achieve sterile cure in patients.[2,3] Therefore, many current TB drug discovery programs focus on strategies to reduce treatment duration, often by prioritizing efforts to inhibit targets other than those already inhibited by current front-line therapies. Because of the historical difficulty of translating the products of target-based medicinal chemistry into compounds with whole-cell activity in the antibacterial field, many drug discovery efforts begin with the target-agnostic process of whole-cell screening for growth inhibition.[4]

Series with whole-cell potency against *Mycobacterium tuberculosis* (*Mtb*) resulting from such screening programs offer an attractive starting point for lead optimization efforts but understanding target novelty requires deconvolution of the molecular mechanism of cell death induced by that series. We have previously proposed whole genome sequencing of resistant mutants as a scalable technique to identify SNPs within potential targets and shown that this works with a small set of screening hits.[5] This methodology works well for small-molecule hits that directly interact with a single protein target but screening hits may, of course, have a more complex mechanism. Even when a single enzyme targeted by a single inhibitor is the predominant mechanism of inhibition of cell growth, whole genome sequencing sometimes gives surprising results that do not immediately provide a clear candidate for the protein target.

Mtb possesses the enzymatic machinery to either synthesize purine nucleotides de novo or scavenge them from the host to provide the essential nucleotides required for DNA synthesis.[6,7] *Mtb* was the first bacterium from which an adenosine kinase activity was identified, and low local concentrations of adenosine are thought to be a feature of at least some tuberculous lesion types.[8,9] The de novo biosynthetic pathway for guanine-containing nucleotides as well as the salvage pathways of purine nucleotides that yield inosine and hypoxanthine as intermediates (Figure 1), all pass through a common intermediate, inosine 5′-monophosphate, to derive the required guanine and adenine containing deoxynucleotide precursors for DNA synthesis. Guanine-containing precursors in particular require conversion of inosine 5′-monophosphate to xanthine 5′-monophosphate through the action of inosine 5′-monophosphate dehydrogenase (IMPDH). *Mtb* encodes three apparent homologues of IMPDH on its chromosome (*guaB1*, *guaB2*, and *guaB3*) but only one (*guaB2*, *Rv3411c*) has been shown to be essential and to catalyze the NAD^+-dependent dehydrogenation and hydrolysis of inosine 5′-monophosphate to xanthine 5′-monophosphate.[10,11] Several series of small-molecule inhibitors of IMPDH have been developed, and recently crystal structures of a truncated form of the *Mtb* enzyme in complex with these inhibitors have appeared.[10,12−14] In general, the whole cell activity of these inhibitors has been only in the 1−10 μM range.

In this work, we identified a novel scaffold that targets IMPDH with low micromolar potency against *Mtb*. The cellular mechanism of this compound was demonstrated by selection of resistant mutants that resulted in amplification of *guaB2* gene expression as well as by the ability of exogenously supplied guanine to rescue their inhibition. We report the kinetics of enzyme inhibition and were able to show by structural analyses that the inhibitor bound to the IMP cofactor in the enzyme active site. Despite the cidality of these IMPDH inhibitors in vitro, this compound had limited efficacy in vivo, and further quantification of guanine in granulomas from infected human and rabbit tissues showed high local concentrations of this nucleotide precursor, limiting the potential of IMPDH as a drug target for *Mtb*.

RESULTS

Identification and Phenotypic Characterization of an Anti-tubercular Indazole Sulfonamide Scaffold. In a screen of 100,000 compounds for inhibitors of growth of *Mtb* (manuscript in preparation), an indazole sulfonamide (**1**) was discovered with low micromolar potency against the organism (Table 1). This compound was attractive from a medicinal chemistry perspective based on its lack of cytotoxicity, acceptable physicochemical properties, high solubility, and synthetic feasibility (Supporting Information; Scheme 1) and acceptable in vitro absorption−distribution−metabolism values (Table S1).

A literature search showed no precedent to guide an understanding of its possible mechanism of action. Because many anti-tubercular drugs in clinical use, and in the drug development pipeline, target aspects of cell wall biosynthesis, we first set out to evaluate this. We had previously developed an assay that measures the extent of up-regulation of the promoter of the *iniBAC* gene cluster, known to be induced by inhibitors of cell wall biosynthesis,[15] by generating a reporter construct where this promoter drives expression of firefly luciferase.[16] Drugs such as isoniazid, ethionamide, SQ109, and ethambutol that inhibit cell wall mycolate or arabinan biosynthesis, increase luciferase expression in the first 48 h of exposure.[16] Initial profiling of

DOI: 10.1021/acsinfecdis.6b00103
ACS Infect. Dis. 2017, 3, 18−33

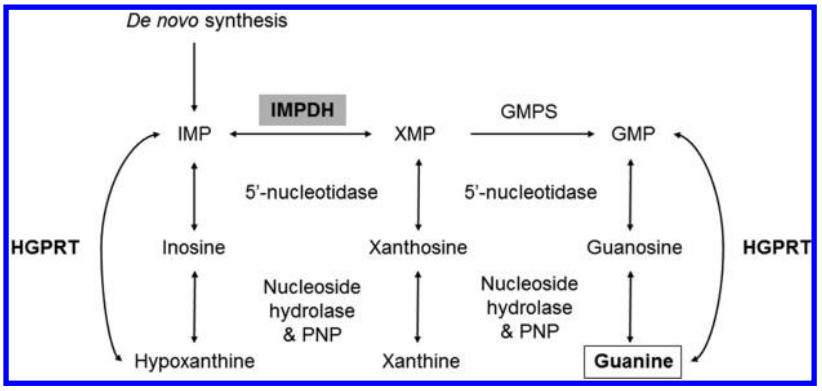

Figure 1. Purine salvage pathway. IMP, inosine monophosphate; GMPS, guanosine monophosphate synthase; XMP, xanthosine monophosphate; GMP, guanine monophosphate; HGPRT, hypoxanthine guanine phosphoribosyltransferase; PNP, purine nucleoside phosphorylase.

Table 1. Indazole Sulfonamides in This Work and Their Antitubercular Potencies[a]

Compound ID	Structure	MIC (μM)[a]
1	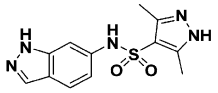	2
2	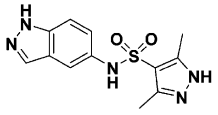	2
3	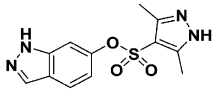	>50
4	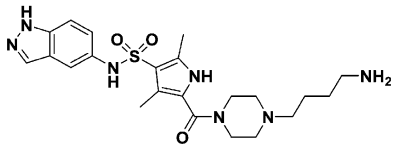	6.2
5	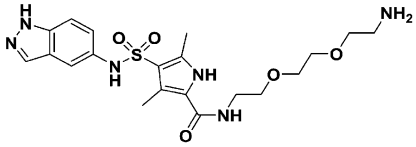	9.5
6	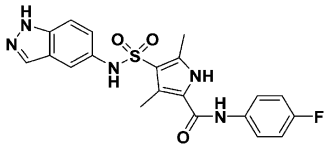	0.09
7	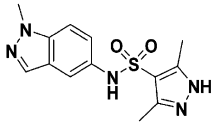	>50

[a]MIC values for compounds **1**–**4** are for *Mtb* H37Rv and for compounds **5**–**7** are for *M. bovis* BCG. MIC for compounds **6** and **7** against *Mtb* H37Rv were 0.2 and >50 μM, respectively.

compound **1** indicated that this promoter was not up-regulated at these early time points, but was up-regulated after 72 h of drug exposure, suggesting a possible downstream effect on cell wall synthesis (Figure 2a). To further confirm an effect on cell wall integrity, we measured the kinetics of extracellular release of an

Scheme 1[a]

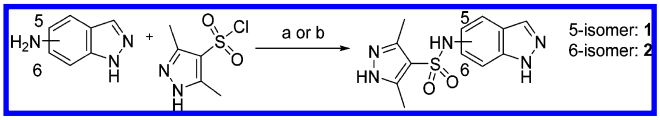

[a]Reagents and conditions: (a) 5- or 6-indazole (1 equiv), sulfonyl chloride (1 equiv), 3,5-lutidine (4 equiv), DCM (2 mL/mmol), 16 h, room temperature. (b) Indazole (1 equiv), sulfonyl chloride (1.2 equiv), pyridine (0.67 mL/mmol), 16 h, 80 °C.

intracellularly expressed green fluorescent protein[17] during compound exposure. Green fluorescent protein (GFP) was released from bacteria, indicating that the compound was lytic, and these effects were observed to be subsequent to the up-regulation of the *iniBAC* promoter (Figure 2b).

To understand better the effects of the indazole sulfonamide on the integrity of the cell wall ultrastructural architecture, we analyzed exposed cells by scanning electron microscopy at time points corresponding to early stages of cell lysis. Compound **1** caused the same polar swelling and cellular elongation observed with β-lactams[17] (Figure 2c). Transmission electron microscopy revealed a similar accumulation of electron-opaque density in the periplasmic region separating the plasma membrane from the outer cell wall layers as had been observed in cells treated with other inhibitors of cell wall biosynthesis[18] (Figure 2c). These results suggested that an aspect of cell wall biosynthesis was inhibited, possibly peptidoglycan. However, a macromolecular incorporation assay using radiolabeled *N*-acetylglucosamine to quantitate effects on peptidoglycan biosynthesis, revealed that compound **1** did not affect incorporation of this precursor into this macromolecule (Figure 2d).

To investigate the effects of the indazole sulfonamide on the metabolism of *Mtb*, we exposed monolayers of cells to increasing concentrations of both an active analogue (**1**) as well as a poorly active sulfonate derivative (**3**) (Table 1) of this compound. Unbiased analysis of the corresponding metabolic pathways indicated that purine metabolism was the most affected pathway with 9 of 92 total enzymatic reactions in this pathway showing perturbations in metabolite pools (Tables 2 and S2). Table 2 shows the detailed results of the pathway analysis obtained using the pathway tool MetaboAnalyst 3.0.[19] Metabolomic analysis of the purine biosynthetic pathway showed that at equimolar concentrations, the active analogue (**1**) resulted in profiles distinct from that of the poorly active derivative (**3**) with marked accumulation of inosine-based nucleotides as well as several pyrimidine- and adenine-based nucleotides (Figure 2a). The concomitant

DOI: 10.1021/acsinfecdis.6b00103
ACS Infect. Dis. 2017, 3, 18–33

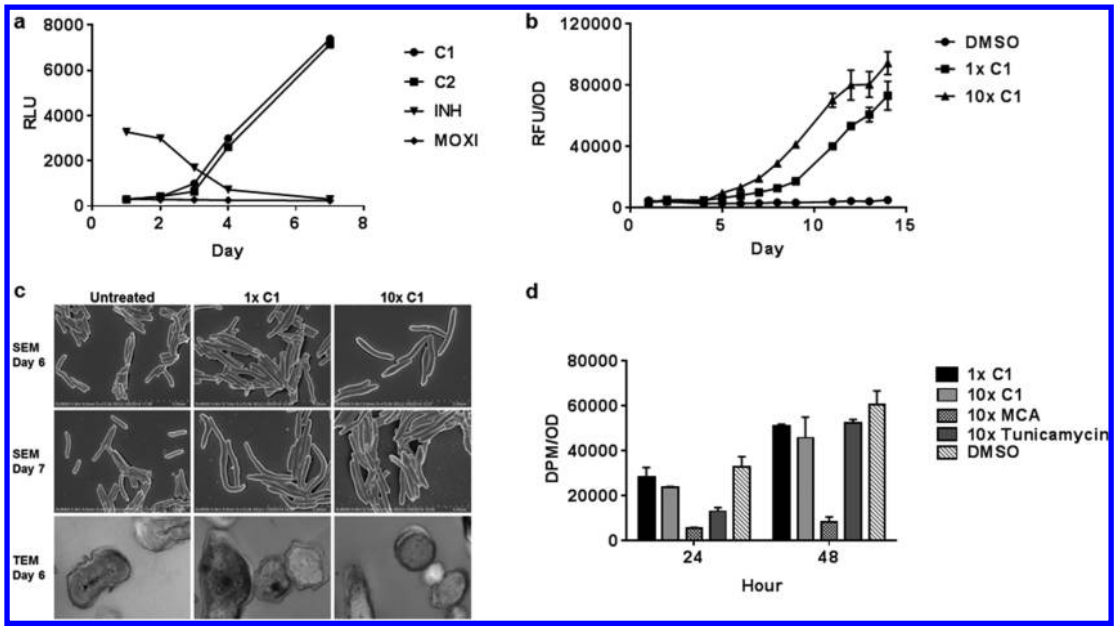

Figure 2. Indazole sulfonamides induce slow lysis of whole cells of *Mtb*. (a) Effects of compounds **1** (C1) and **2** (C2), isoniazid, and moxifloxacin at their MIC concentrations on expression of the cell wall responsive *iniBAC* promoter as measured using the *pini-luc* strain. (b) C1 results in release of cytosolic proteins as measured by GFP-based fluorescence in culture supernatant during exposure to the compound. (c) Scanning (rows 1 and 2) and transmission (row 3) electron microscopy of untreated or C1 exposed cells at 1× (column 2) or 10× MIC values. (d) The indazole sulfonamides do not inhibit peptidoglycan biosynthesis at 1× and 10× MIC concentrations as measured by radiolabeling of the macromolecule using ^{14}C-*N*-acetyl-D-glucosamine. The positive controls meropenem/clavulanate (MCA) and tunicamycin were used at 10× MIC values.

Table 2. Pathway Enrichment Analysis of Compound 1 on the *Mtb* Metabolome

pathway	hits[a]	total[b]	raw *p* value[c]	Holm-adjusted *p* value[d]	FDR[e]
purine metabolism	9	92	3.9×10^{-8}	3.16×10^{-6}	3.16×10^{-6}
lysine biosynthesis	4	32	0.00016	0.012	0.006
arginine/proline metabolism	4	77	0.0046	0.356	0.122
pyrimidine metabolism	3	60	0.016	1	0.312
alanine, aspartate, and glutamate metabolism	2	24	0.019	1	0.312
amino sugar and nucleotide sugar metabolism	3	88	0.044	1	0.587

[a]Actual number of matched compounds within the associated pathway. [b]Total number of compounds in the pathway the column labeled "hits" indicates. [c]Original/uncorrected *p* value calculated from the enrichment analysis. [d]*p* value adjusted by Holm−Bonferroni method. [e]*p* value adjusted using the false-discovery rate.

decrease in xanthosine monophosphate led us to examine the dose-dependent effects of compound **1** on intracellular inosine monophosphate (IMP), xanthosine monophosphate (XMP), and guanine monophosphate (GMP), which showed that the accumulation of IMP was inversely associated with concentrations in XMP and GMP pools (Figure 3b).

Mutants with Acquired Resistance Suggest *guaB2* Overexpression. We selected for mutants that were spontaneously resistant to 10-fold minimum inhibitory concentration (MIC) levels of compounds **1** and **2** (Table 1) on solid media and found that these appeared at a frequency of 1×10^{-9}. These mutants were subsequently confirmed to be 8- and >32-fold resistant to the sulfonamide scaffold (Table 3). Whole genome sequencing of two mutants that were obtained revealed that, although both had single-nucleotide polymorphisms (SNPs) in *nadD* (encoding the nicotinate-nucleotide adenylyltransferase), one mutant had a SNP in the likely promoter region of *guaB2* (*Rv3411c*), whereas the other mutant had an approximately 20-fold duplication of a 50kb genomic region spanning from *Rv3371* to *Rv3411c* (Figure 4a; Table 3).

Using the available X-ray crystal structure of NadD in complex with NADP (PDB ID: 4YBR), we analyzed the effects of the predicted NadD amino acid substitutions on the protein structure and function using a previously established pipeline.[20] V14 is located at the dimer interface between the two NadD protomers, making local hydrophobic intra- and intermolecular interactions. Mutation to isoleucine is not predicted by SDM[21] and DUET[22] to affect the stability of the protomer. There is sufficient space at the interface to accommodate the isoleucine and maintain the hydrophobic interactions, and accordingly this mutation is not predicted by mCSM-PPI[23] to destabilize the homodimer. V14 is located 8 Å from the NAD ligand, and mutation to isoleucine is predicted by mCSM-lig[24] to mildly decrease binding affinity. G180A is a surface mutation of a negative phi glycine on an α-helix of NadD, which SDM and DUET do not predict will destabilize the protomer, and mCSM-PPI predicts this change will have minimal effect on formation of the homodimer. The mutation is located 16.6 Å from the NAD binding site and is predicted by mCSM-lig to have minimal effect on the affinity for NAD. This suggested that these mutations were unlikely to play a direct role in the resistance observed to these compounds.

Quantitative PCR confirmed the 20-fold amplification of the *Rv3371*−*Rv3411* spanning region originally observed in the whole genome sequencing (Figure 4b), and quantitative RT-PCR analysis confirmed that the SNP in the promoter of *Rv3411c* caused up-regulation of *guaB2* transcript expression (Figure S1). Quantitative PCR of genomic DNA of the mutant compared to the parental strain showed that this gene was amplified 14-fold in

DOI: 10.1021/acsinfecdis.6b00103
ACS Infect. Dis. 2017, 3, 18−33

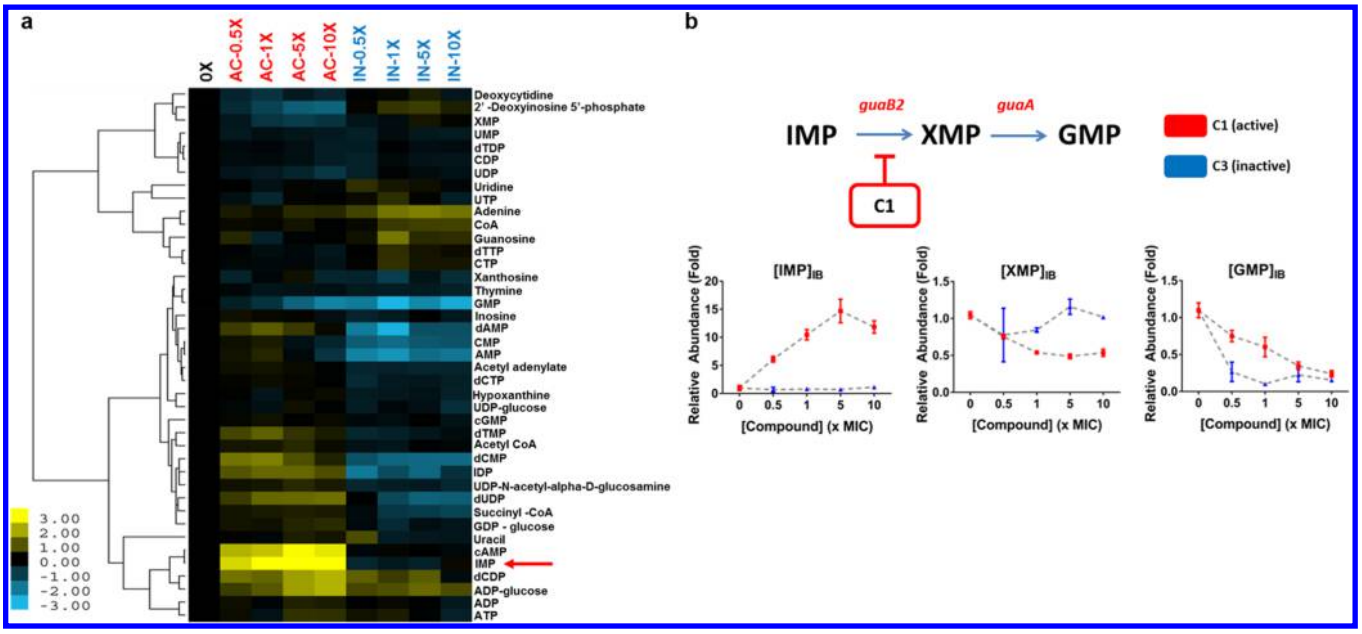

Figure 3. Indazole sulfonamides induce accumulation of IMP and reduction of XMP and GMP levels. (a) Heatmap of intracellular metabolite concentrations in purine metabolism as a function of concentration of active (AC) and inactive (IN) analogues **1** and **3**, respectively. Cells were treated with analogues at equimolar concentrations corresponding to 0, 0.5, 1, 5, and 10× MIC values of compound **1**. (b) Compound **1** results in dose-dependent intrabacterial (IB) accumulation of IMP with concomitant decreases in XMP and GMP metabolite pools likely as a result of IMPDH inhibition.

Table 3. Mutation of Indazole Sulfonamide Resistant Mutants

ID	deletions	duplications	SNPs	MIC (fold)
SR2.1	*plcD* *Rv1787−Rv1790*	∼20-fold duplication of *Rv3371−Rv3411c*	*nadD*:G180A	32−64
SR2.2	none	none	*nadD*:V14I, *nrdZ*:C67F G>A: −49 bp of *Rv3411c*	8

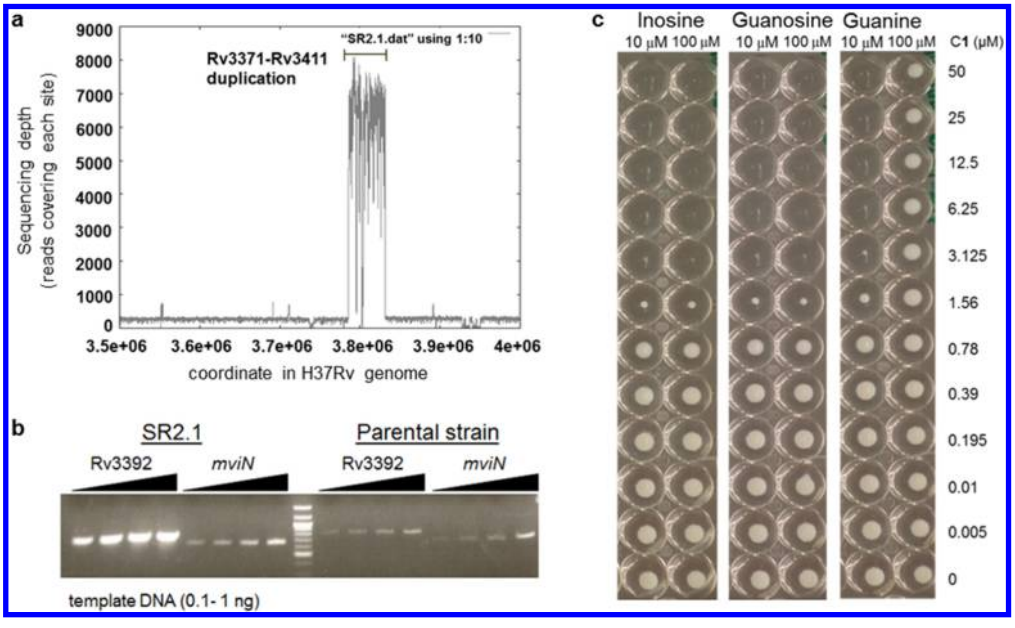

Figure 4. Resistance to the indazole sulfonamides develops through an unusual gene amplification of a 40 gene region that includes IMPDH. (a) Density of reads across the genome as measured by Illumina-based sequencing. (b) Quantitative PCR analysis of *Rv3392* inside the amplified region as compared to *mviN* (control outside the amplified region) in the SR2.1 sulfonamide resistant mutant as compared to parental strain showing >10 amplification. (c) Guanine, but not guanosine or inosine, rescues growth inhibition by compound **1**.

the genome of the resistant mutant (results not shown). We reasoned that if the mechanism of growth inhibition involved the essential *Mtb* IMPDH encoded by *guaB2* that catalyzes NAD^+-dependent oxidation of IMP to XMP in the de novo biosynthetic

DOI: 10.1021/acsinfecdis.6b00103
ACS Infect. Dis. 2017, 3, 18−33

pathway for guanosine nucleotides, growth inhibition would be overcome by guanine supplementation.[25] Guanine rescue would only be possible in the presence of a functional purine salvage pathway in the cell conferred by the hypoxanthine−guanine phosphoribosyltransferase (HGPRT) encoded by the *hpt* gene that phosphoribosylates hypoxanthine or guanine to replenish purine nucleotide pools.[26] Indeed, concentrations of guanine above 100 μM rescued cells from the effects of **1** and **2** (Figure 4c; Table S3), showing that the salvage pathway utilizing the activity of HGPRT could overcome metabolic blockage of IMPDH. In contrast, guanosine and the IMPDH substrate inosine could not rescue growth, likely due to lack of uptake mechanisms of these nucleosides (Figure 4c). As expected, no other nucleobases could rescue *Mtb* from indazole sulfonamide (results not shown).

Indazole Sulfonamides Are Uncompetitive Inhibitors of IMPDH. We next confirmed the ability of this compound to inhibit *Mtb* IMPDH in vitro. Recombinant *Mtb* IMPDH was expressed as a truncated isoform of the catalytically active core after deletion of both cystathione β-synthase (CBS) domains,[27] with no alteration on its steady state kinetic constants when compared to native *Mtb* IMPDH.[12] Compound **1** displayed an IC_{50} of 0.38 ± 0.02 μM (r^2 = 0.99) in the enzyme assay (Figure 5a). Moreover, comparison of in vitro enzyme inhibition values to potency of analogues (manuscript in preparation) against whole cells showed remarkable correlation (r^2 = 0.8) (Figure 5b).

To further confirm target engagement in the context of the cellular environment, a chemoproteomic approach was used to identify potential binding partners from the mycobacterial proteome.[28] This strategy is based on the immobilization of chemical analogues of the active compound to beads, which are subsequently incubated with bacterial extract. Proteins captured by the beads were identified after tryptic digestion and liquid chromatography−tandem mass spectrometry (LC-MS/MS). We prepared indazole sulfonamide analogues, which derivatized the active pharmacophore with different types of linkers and a primary amino group, allowing covalent attachment to Sepharose beads. Compound **5** retained antibactericidal activity (Table 1), suggesting that the derivatization with the linker moiety did not interfere with target binding. The derivatized beads were incubated with *Mycobacterium bovis* BCG extract, and proteins captured by the beads were digested with trypsin, labeled with isobaric mass tags (TMT 10plex) and quantitatively identified by LC-MS/MS. To distinguish true targets from nonspecific background binding, aliquots of the bacterial extracts were incubated prior to the pulldown step with either the antibacterial compound **6** or with the structurally related inactive compound **7** (Table 1). The active compound, but not the inactive analogue, is expected to bind to the target protein(s) in the lysate and thus reduce the binding of these proteins to the beads. IMPDH (BCG_3481c, GuaB2) was the only protein in our experiments that exhibited this behavior, suggesting that the active compound is a selective IMPDH inhibitor (Figure 5c). The inactive compound **7** showed only partial competition of bead binding with IMPDH even at the high concentration of 40 μM (Figure 5d). GuaB1 and GuaB3 were captured by the beads to some degree, but this binding was not affected by excess compound **6**, suggesting that they are not targets of compound **6**. To estimate inhibitor potency, we performed the pulldown step in the presence of different concentrations of "free" compounds, which allowed

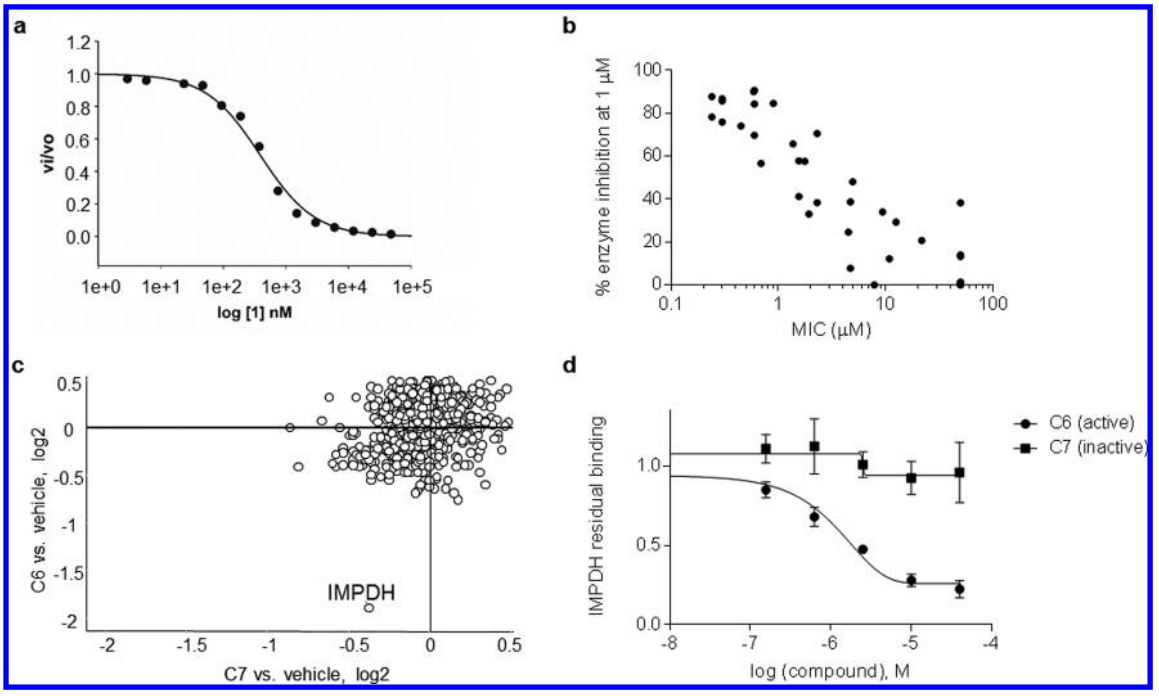

Figure 5. Indazole sulfonamide inhibits *Mtb* IMPDH. (a) Kinetics of *Mtb* IMPDH inhibition. (b) Correlation between *Mtb* IMPDH inhibition and potency against *Mtb* cells as measured by MIC. (c) Identification of IMPDH as a target by chemoproteomics. Compound **5** was covalently immobilized to NHS-activated Sepharose beads at the primary amine. The beads were incubated with *M. bovis* BCG extract either in the presence of vehicle (DMSO) or in the presence of compound **6** (active) or the inactive analogue compound **7**. Relative quantification of all proteins captured on the beads was performed by isobaric peptide tagging and LC-MS/MS. A single protein, IMPDH (BCG_3481c, GuaB2), showed specific and selective binding as indicated by loss of binding in the presence of excess compound **6**, but not compound **7**. (d) Affinity capturing on beads in the presence of different concentrations of "free" compounds allowed the determination of an IC_{50} value of 0.8 μM and an apparent dissociation constant (K_d^{app}) of compound **6** for IMPDH, whereas compound **7** shows only very weak binding. Data shown are the results of two replicate experiments.

DOI: 10.1021/acsinfecdis.6b00103
ACS Infect. Dis. 2017, 3, 18−33

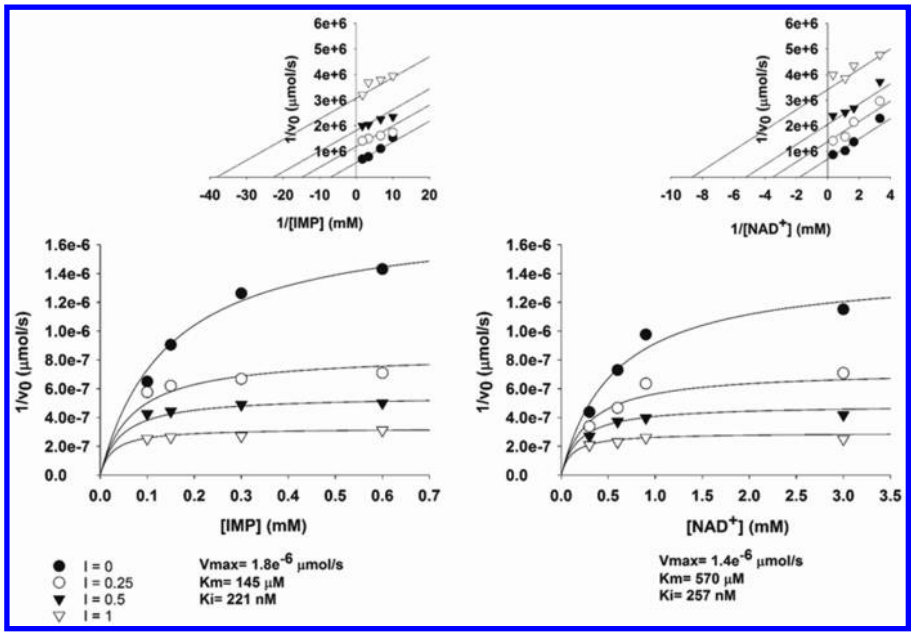

Figure 6. Indazole sulfonamide is an uncompetitive inhibitor of *Mtb* IMPDH: the mechanism of inhibition of compound **1**. Lineweaver–Burk plots (upper) were generated to display the type of inhibition, which is uncompetitive for both IMP and NAD^+.

the determination of an IC_{50} value of 0.8 μM for IMPDH. The IC_{50} value represents a measure of target affinity, but is affected by the affinity of the target for the bead-immobilized ligand. The latter effect can be deduced by measuring the depletion of the target protein by the beads.[29] The apparent dissociation constant (K_d^{app}) of compound **6** for IMPDH was determined to be 0.7 μM. To exclude potential adverse effects mediated by modulation of host (human) targets, we employed the same strategy to evaluate binding to proteins in extracts from human material (K562 erythroleukemia cells, HEK embryonic kidney cells, and placenta tissue). Notably, the human orthologues IMPDH1 and IMPDH2 were captured by the indazole sulfonamide beads, but were not affected by pre-incubation with excess "free" compound **6**, indicating a high degree of selectivity for the bacterial over the human enzyme.

The mode of enzyme inhibition is critical in evaluating the potential of a compound as a growth inhibitor in vivo because the extent of inhibition of the reaction can be determined by substrate and/or product concentrations depending on inhibitor kinetics. Kinetic evaluation of compound **1** showed the mode of inhibition was uncompetitive with IMP and NAD^+ (Figure 6) with a K_i of 0.220 μM. Uncompetitive inhibitors are appealing in that enzyme inhibition could lead to a buildup of substrate, further driving enzyme inhibition. In addition, the IC_{50} of compound **1** against the human IMPDH was found to be 15 μM (Figure S2), showing a selectivity index of approximately 40 for the *Mtb* IMPDH.

X-ray Structure of Indazole Sulfonamide, Compound 1, and IMPDH. The *Mycobacterium thermoresistible* (*Mth*) IMPDH protein, which shares 85% amino acid identity with the *Mtb* IMPDH, including a 100% conservation of residues in the active site, was chosen for structural studies because it gave higher protein expression yields than the *Mtb* homologue. *Mth* IMPDH ΔCBS crystallized in the *I*4 space group and diffracted to sub 2 Å resolution. One protomer was present in the asymmetric unit, with the biological tetramer observable through operation of 222 symmetry of the crystal lattice (Figure 7a). In the X-ray crystal structures of compound **1** with *Mth* IMPDH, clear electron density for the compound was observed within the NAD binding pocket of IMPDH in the $2F_0 - F_c$ difference map ($\sigma = 3.0$), stacking with IMP (Figure 7b,c). It is worth noting that the majority of interactions mediated by compound **1** within the crystal structure are through extensive pi interactions between the indazole group and the hypoxanthine group of IMP (Figures 7e and S3) consistent with the uncompetitive binding mode suggested by the enzyme kinetics. The indazole is able to make further pi interactions with A285 (A269 in the *Mth* structure) and polar interactions with G334 and T343 (G318 and T327 in the *Mth* structure, respectively). The pyrazole makes further pi interactions to A269, in addition to some proximal hydrophobic interactions to E458 (E442 in the *Mth* structure). Additional polar interactions are mediated by the sulfonyl group to G425 (G409 in the *Mth* structure).

From crystals soaked with compound **6**, the $2F_0 - F_c$ difference map ($\sigma = 3.0$) revealed strong density for the inhibitor (Figure 7d). The structure of compound **6** showed the compound bound in a nearly identical manner to compound **1** (Figure S3), with the indazole sulfonamide taking advantage of the same extensive interactions to IMP, in addition to a few interactions with neighboring residues in the binding pocket (A285, G334, T343, G425, and E458). The fluorophenyl acetamide extension of compound **6** is able to make polar interactions with T284, A285 and H286 (T268, A269, and H270 in the *Mth* structure, respectively) and the benzene group making proximal hydrophobic interactions to H286, N289, and V292 (H270, N273, and V276 in the *Mth* structure, respectively). Notably, however, the fluorine is in good orientation to make a 3.2 Å hydrogen bond with the side chain of N289, helping to lock in the orientation of the compound.

Indazole Sulfonamides Are Growth Dependent Inhibitors of Mtb. Having confirmed the on-target inhibition of IMPDH both in vitro and in the context of cellular metabolism, we explored the physiological consequences of IMPDH inhibition on *Mtb* survival. Exposure of *Mtb* to compounds **1** and **2** showed that IMPDH inhibition resulted in slow bacterial death at high concentrations, whereas MIC levels of compounds resulted

DOI: 10.1021/acsinfecdis.6b00103
ACS Infect. Dis. 2017, 3, 18–33

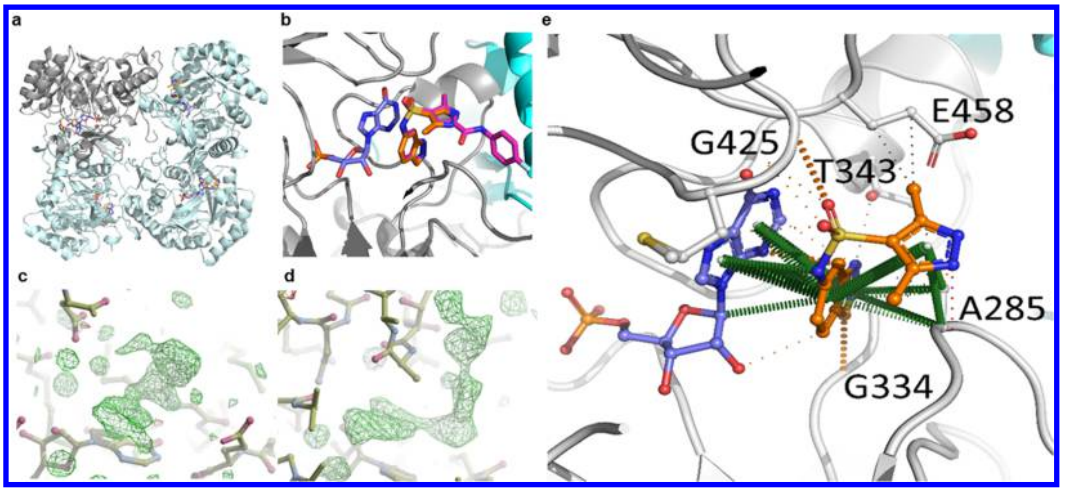

Figure 7. X-ray crystal structure of compounds **1** and **6** bound to IMPDH. (a) IMPDH tetramer (cyan ribbon, with a representative protomer shown in gray) is shown bound to IMP (blue) and **1** (orange) is shown. (b) Structural alignment of the IMPDH crystal structures of **1** (orange) and **6** (magenta), showing the inhibitors are orientated identically in the NAD^+ binding pocket. (c, d) $2F_0 - F_c$ difference maps ($\sigma = 3.0$) showing clearly visible electron density for **1** (c) and **6** (d) in the NAD^+ binding site. (e) Interactions made by **1** (orange) in the X-ray crystal structure of the complex of IMPDH (gray; and adjacent protomer in cyan) with IMP (blue). Residue numbering is of the corresponding residues in *Mtb*. Pi interactions are shown in green, hydrogen bonds in red, polar interactions in orange, and proximal hydrophobic interactions in gray. The solid lines are covalent bonds, and the dashed lines are noncovalent interactions.

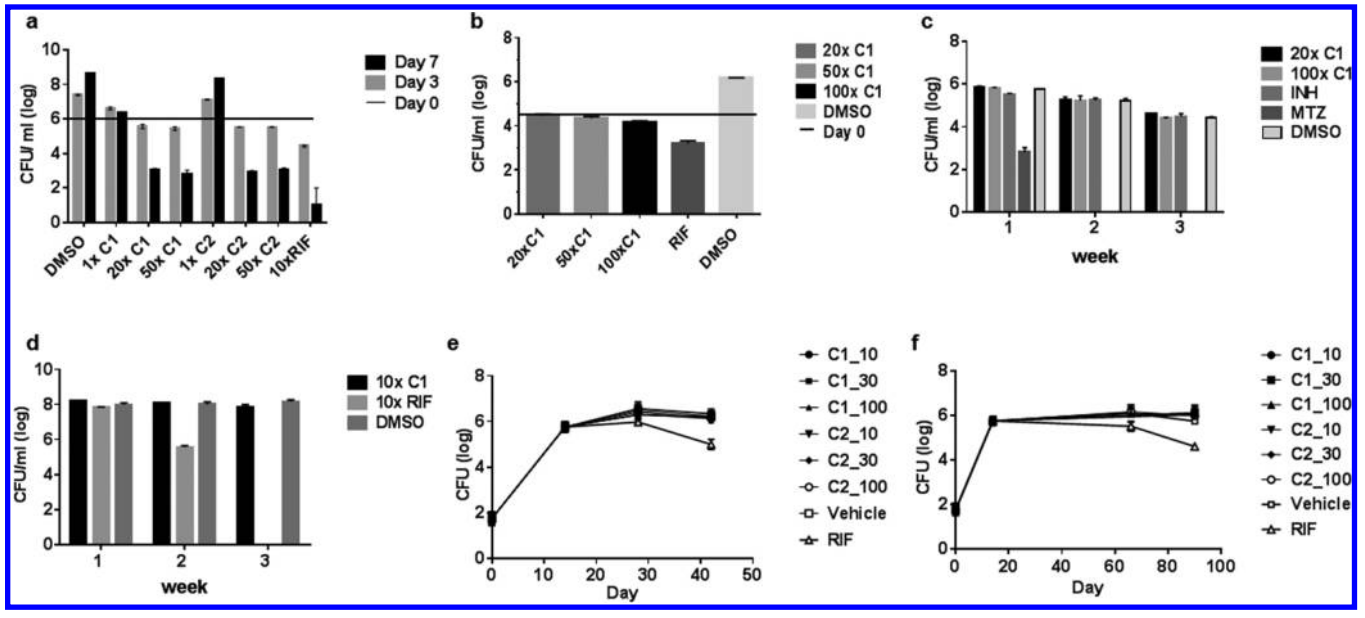

Figure 8. Indazole sulfonamide is cidal for replicating cells but lacks activity in nonreplicating cells and in murine infection. (a) Logarithmically growing *Mtb* was exposed for 7 days to compounds **1** (C1) and **2** (C2) at 1, 20, and 50× MIC values. Control cells were exposed to 10× MIC concentrations of rifampicin (RIF). (b) **1** lacks cidality against *Mtb* during growth in macrophages. *Mtb*-infected J774 macrophages were exposed to C1 at 10, 50, and 100× MIC concentrations for 7 days prior to CFU enumeration. RIF and DMSO were used as positive and negative controls, respectively. (c) **1** is inactive against anaerobically persisting cells. Anaerobically adapted cells were exposed for up to 3 weeks to **1** at 20 and 100× MIC values prior to CFU enumeration. Metronidazole at 100 μM was used as positive control. Isoniazid (100 μM) and DMSO were used as negative controls. (d) **1** lacks efficacy against starved nonreplicating *Mtb*. Two-week starved *Mtb* cultures were exposed for up to 3 weeks to **1** and RIF at 10× MIC values prior to CFU enumeration. **1** lacks efficacy in acute (e) and chronic (f) stages of murine infection as measured by CFU analysis of lung tissues. Mice were dosed at 10, 30, and 100 mg/kg of **1** and **2** with vehicle and 10 mg/kg RIF treated mice serving as negative and positive controls, respectively.

only in bacterial growth inhibition (Figure 8a). The kinetics of cidality recapitulated the late up-regulation of the cell wall responsive *iniBAC* promoter and bacterial lysis observed during treatment of *Mtb* with these compounds (Figure 2a). We confirmed that these compounds exerted a growth inhibitory effect in macrophages (Figure 8b), although high concentrations were required to affect bacterial stasis. The vulnerability of IMPDH during nonreplicative bacterial persistence in vitro was determined by treating starved or anaerobically adapted *Mtb* with compound **1** or **2**, which showed that exposures as long as 3 weeks at 100-fold MIC levels of compound did not significantly affect bacterial survival (Figure 8c,d), arguing against the vulnerability of this target during nonreplicating persistence. These results suggest that IMPDH inhibitors were only effective against replicating *Mtb* cells.

To establish the vulnerability of IMPDH during host pathogenesis, we first sought to verify the efficacy of these compounds in an animal model that supports *Mtb* replication. *Mtb* replicates

DOI: 10.1021/acsinfecdis.6b00103
ACS Infect. Dis. 2017, 3, 18−33

in lungs of both acute as well as chronically infected C57BL/6 mice, in chronic stages of infection replication being balanced by bacterial death.[30] *Mtb*-infected C57BL/6 were treated with 10−100 mg/kg of **1** and **2** with dosing initiated 2 weeks post-infection as well as in 7-week-infected mice, in which a chronic infection had been established. Our results showed a surprising lack of efficacy in both stages of infection as observed by a lack of effect on bacterial organ burdens compared to treatment controls (Figure 8e,f).

Factors That Contribute to Lack of in Vivo Efficacy. The lack of in vivo efficacy of the indazole sulfonamide contrasted with its in vitro efficacy and led us to explore the factors that contributed to this. The finding that guanine could rescue the cidality in vitro (Figure 4C, Table S3) could suggest that the pathogen employed scavenging mechanisms for host derived guanine similarly to the scavenging of host derived nicotinamide in NAD salvage observed during growth in macrophages.[31] Labeling of cells growing axenically in vitro or released after growth in macrophages[31] with radiolabeled guanine indicated that guanine uptake mechanisms were downregulated during parasitism of the host (Figure 9A) as compared to rapidly in vitro replicating cells, arguing against increased salvage of host purines contributing to the discrepancy between in vitro and in vivo efficacy.

We next sought to understand whether inhibitor concentrations at the site of infection could have played a role in the lack of in vivo efficacy. We analyzed the compound exposure required to effect bacterial killing in vitro and during infection of host macrophages by daily addition and removal of drug after either 3 or 6 h of drug exposure compared to constant exposure (24 h). These studies suggested that continuous exposure at 10-fold MIC values was required to exert a cidal effect in vitro (Figure 9b) and stasis in macrophages (Figure S4). Analysis of the guanine concentration required to rescue growth inhibition demonstrated that concentrations of 10 μM guanine showed partial rescue of growth in an indazole sulfonamide concentration-dependent manner, whereas 100 μM could fully overcome all growth inhibition (Figure S5).

Pharmacokinetic analysis of blood concentrations of the two indazole sulfonamides (compounds **1** and **2**) used for treatment of infected mice in Figure 8e,f showed that, although the highest dose achieved a maximal serum concentration >10-fold higher than MIC values and an area-under-the-curve (AUC) value >30-fold higher than MIC values (Figure 9c), the compound was well below the effective cidal concentration after 8 h of dosing. The AUC following oral pharmacokinetics (PK) showed that for compound **1** there was a proportional increase as the dose was escalated, whereas for compound **2** there was a proportional increase between 5 and 30 mg/kg but not between 30 and 100 mg/kg as the exposure was moderate when compared to each other (Table S11). Analysis of drug concentrations for compound **1** in bronchoalveolar lavage analyses similarly showed that despite drugs reaching high concentrations in the epithelial lining fluid, concentrations at 4 h after dosing were below the efficacious concentration and a reflection of the free drug concentration in blood (Tables S11 and S12). Moreover, analysis of permeability and efflux of this scaffold in a Madin Darby canine kidney cell permeability assay indicated that this scaffold was a likely P-glycoprotein (P-gp) substrate (Figure 9d), which could additionally have contributed to low microenvironmental concentrations of these compounds in the mouse lung.

Our result suggested that efficacy in the mouse model could be improved by developing a compound with better serum exposure and lower P-gp efflux. However, the finding that

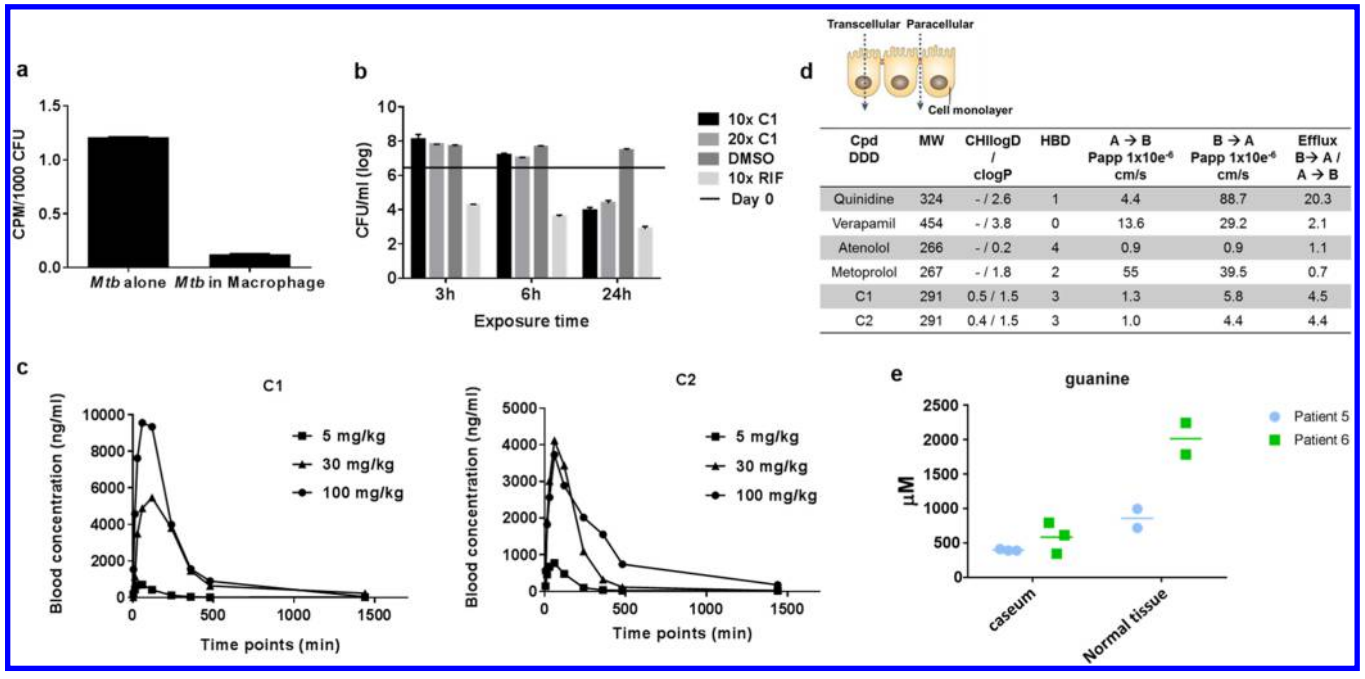

Cpd DDD	MW	CHIlogD / clogP	HBD	A → B Papp 1x10^{-6} cm/s	B → A Papp 1x10^{-6} cm/s	Efflux B→ A / A → B
Quinidine	324	- / 2.6	1	4.4	88.7	20.3
Verapamil	454	- / 3.8	0	13.6	29.2	2.1
Atenolol	266	- / 0.2	4	0.9	0.9	1.1
Metoprolol	267	- / 1.8	2	55	39.5	0.7
C1	291	0.5 / 1.5	3	1.3	5.8	4.5
C2	291	0.4 / 1.5	3	1.0	4.4	4.4

Figure 9. Failure to achieve murine efficacy is likely due to suboptimal exposure, P-GP-mediated efflux, and high lesion guanine levels. (a) *Mtb* does not up-regulate guanine uptake during host pathogenesis. *Mtb* growing in macrophages was compared to logarithmically growing cells for their radiolabeling by ^{14}C-guanine. (b) Extended exposure of *Mtb* to compound **1** (C1) at 10 and 20× MIC concentrations is required to effect cidality. Logarithmically growing *Mtb* was exposed for 7 days to compounds for daily exposure periods of 3, 6, or 24 h followed by compound removal. (c) Pharmacokinetics of **1** and **2**. (d) Measurement of permeability and efflux of **1** and **2** in a Madin Darby canine kidney cell permeability assay. (e) Guanine concentrations in microscopically unaffected tissue and in lesions in resected lung tissue from two tuberculosis patients.

DOI: 10.1021/acsinfecdis.6b00103
ACS Infect. Dis. 2017, 3, 18−33

guanine concentrations determine the efficacy of an IMPDH inhibitor in vitro led us to explore guanine concentrations in lung tissue. *Mtb*-infected rabbits develop granulomas with many of the defining characteristics of human granulomas.[32] Dissecting caseous lesions from *Mtb*-infected rabbits allowed quantitation of free guanine levels in rabbit caseum directly and revealed guanine concentrations in the range of 0.2−0.5 mM both in uninvolved lung tissue and in lesions in rabbits that is greater than the 0.1 mM guanine required for rescue (Figure S6). Similarly, curated samples of human tissue from patients with refractory multidrug-resistant tuberculosis who had undergone surgical resection for the treatment of their disease were analyzed for guanine content. Granuloma and cavity caseum had between 0.4 and 0.8 mM guanine, and visually uninvolved lung tissue from the same two patients had 2−3 times more guanine than present in the lesion tissue (Figure 9e). In contrast, J774 cells had guanine concentrations (43 μM) in the range of that reported for subpopulations of human cells,[33] whereas the guanine concentrations in mouse tissues ranged from 7 to 20 μM (Table S13; Figure S7), concentrations that could partially rescue growth inhibition (Figure S5).

DISCUSSION

The *iniBAC* promoter is a reporter of cell wall insult that rapidly responds to broad classes of cell wall inhibitors within 24 h.[15,16] In the case of the indazole sulfonamides we initially classified them as not cell wall active on the basis of the absence of this response but noted with interest that these compounds induced cell lysis and resulted in a delayed firing of the *iniBAC* promoter. We had seen a similar pattern of in vitro behavior previously with meropenem, a β-lactam of the carbapenem family. In this case this phenotype was accompanied by a unique polar swelling visualized by electron microscopy.[17] The indazole sulfonamides showed a similar swelling at the cell poles but did not exhibit any direct effect on incorporation of ^{14}C-*N*-acetylglucosamine, a precursor to peptidoglycan, suggesting that they did not exert a direct effect on peptidoglycan biosynthesis despite these similarities to β-lactams. The metabolic profiles resulting from treatment of *Mtb* cells with the indazole sulfonamides strongly suggested an effect on purine nucleotide pools, suggesting that the cell wall effects were downstream consequences of purine nucleotide pool perturbations.

Mutants resistant to the indazole sulfonamides proved remarkably difficult to select and occurred only at very low frequency. Sequencing of these mutants at first revealed no helpful SNPs to suggest the actual target; instead, we observed a 2−20-fold tandem duplication of a nearly 50 kb pair region of the chromosome spanning 40 genes from *Rv3371* to *Rv3411c*. Remarkably, large-scale repeats of genes in this region of the chromosome have been reported in the Pasteur strain of BCG, the Beijing strain of *Mtb*, and more recently in several other modern TB lineages.[34−36] The only resistant mutant we obtained that did not show this gene amplification harbored a SNP just upstream of the last gene in the amplified region, *guaB2*. The finding that guanine supplementation rescued *Mtb* from growth inhibition by this scaffold confirmed the notion that the mechanism of action was related to inhibition of IMPDH.

The connection between IMPDH inhibition and the observed effects on cell envelope integrity was unexpected, but three facts are worth considering. The observed cell lysis occurs very slowly and only after about 5 days, with the *iniBAC* promoter assay becoming positive slightly earlier at about 3 days. The central role of guanine nucleotides in protein synthesis and biosynthesis of the essential flavin cofactor required for a plethora of reactions including UDP-galactopyranose mutase could additionally explain the downstream effects on cell wall integrity.

The very low observed frequency of resistance suggested the possibility that there were multiple cellular targets for the indazole sulfonamides. Two experiments suggest that this is not the case. First, across a structurally diverse set of analogues of this series with MICs ranging from 100 nM to 100 μM, the IC_{50} values against IMPDH showed a strong correlation. Second, attachment of an indazole sulfonamide analogue to beads specifically pulled IMPDH out of whole cell lysates, and this could compete with an active analogue but not with a closely related inactive analogue (Figure 5c). A more likely explanation for the low frequency of resistance appeared when we solved the X-ray crystal structure of our lead compound in complex with the IMPDH from *M. thermoresistible*. Full-length *Mth* IMPDH (GuaB2) has 85% sequence identity with *Mtb* IMPDH, is 100% conserved in the active site, and was chosen for further crystallographic studies due to its higher expression levels and ready crystallization in a soakable crystal form. This structure showed that the inhibitor bound primarily to the substrate IMP at the active site and made relatively few contacts with the protein. The relative lack of direct interaction with the protein itself suggests that mutation of the target is unlikely to give resistance, leaving gene amplification as the only viable route for acquisition of resistance. This gene amplification may occur at an even lower rate in vivo because amplification of this region in vitro leads to mutants with impaired virulence.[37] The two nonactive site mutations observed in *nadD*, encoding the nicotinate mononucleotide adenylyltransferase involved in NAD biosynthesis, in our resistant mutants are intriguing. We have confirmed that our compound even at 100 μM does not inhibit MtNadD, further corroborating the notion that these non-active-site mutations are not related to the mechanism of action of the compound.

Consistent with their induction of cell lysis, the indazole sulfonamides were cidal to actively replicating cells over a 1 week incubation. Consistent with the anabolic role of the products of this enzyme, this series showed no significant cidal activity against cells in which replication had been arrested by hypoxia. We therefore expected to see an effect of these compounds in acute murine models of disease and for that activity to be significantly curtailed in chronic disease models, where replication is slow. Surprisingly, we saw no activity of these agents in either model despite what appeared to be suitable exposures. We considered several explanations for the lack of in vivo activity including that the bacteria might have up-regulated their ability to scavenge guanine derived from the host and therefore be less susceptible to IMPDH inhibitors. Uptake of [^{14}C]-guanine, however, was not up-regulated in *Mtb* cells released from macrophages compared to those in in vitro culture. Cidal activity was very concentration dependent, and at the actual MIC, the compounds were sufficient to block replication, but killing was only apparent above 10× MIC concentrations. To mimic the exposures seen in vivo, we next assessed what duration of exposure was required to achieve cidal activity and did daily pulses of exposure for 3, 6, or 24 h at 20× MIC and found that even 6 h at 20× MIC was insufficient to kill cells. We also found that these compounds were subject to active efflux by P-gp, so the actual exposure of bacteria within macrophages was likely considerably lower than what was measured in the serum PK study.

Another potential explanation for the lack of in vivo efficacy was that host guanine levels were sufficient to rescue the IMPDH inhibitory effect. To assess this, we measured free guanine levels

DOI: 10.1021/acsinfecdis.6b00103
ACS Infect. Dis. 2017, 3, 18−33

in mouse, rabbit, and human TB lesions and found surprisingly high concentrations of guanine in normal lung tissue as well as in the caseum of granulomas of rabbits and humans, whereas normal lung tissue of uninfected mice was 10−13 μM. High intracellular concentrations of guanine have previously been reported in both *E. coli*[38,39] (∼180 μM) and normal human cells[33] (70−800 μM). Intracellular guanine concentrations in J774 macrophages used in our work were measured to be 43 μM, levels not high enough to fully rescue growth inhibition by the indazole sulfonamide, although high enough to partially alleviate cidality. Although the mouse lung concentrations do not explain the lack of efficacy in this animal model, these levels are a concern for IMPDH as a drug target in humans where salvage of extracellular guanine could provide a bypass mechanism for decreased flux through the de novo pathway (Figure 1). The most recalcitrant bacteria are thought to be the nonreplicating bacilli found within the necrotic core of lesions where guanine was the lowest but where the metabolic requirement for guanosine nucleotides is minimal as evidenced by the growth rate dependence of IMPDH inhibition. In combination, these data suggest that IMPDH, although essential for *Mtb* survival in vitro in laboratory growth media, is relatively invulnerable and has low potential for achieving treatment shortening in humans infected with *Mtb*.

MATERIALS AND METHODS

Animal Care and Human Ethics Assurance. Mouse and rabbit studies were carried out in accordance with the Guide for the Care and Use of Laboratory Animals of the National Institutes of Health under Animal study protocol numbers LCID 4E and LCID 3; additional rabbit studies were done with approval from the Institutional Animal Care and Use Committee of the New Jersey Medical School, Newark, NJ, USA, under Rutgers Animal Welfare Assurance No. A3158-01. For human samples, anonymized lung tissue containing granulomas were collected from patients with treatment refractory TB during therapeutic lung resection surgery at National Masan Hospital, Republic of South Korea. The collection was approved by the hospital's institutional review board, an exemption from National Institutes of Health, Office for Human Research Protections, and with written, informed consent of the subjects. All regulated procedures on living animals performed at the University of Dundee were carried out under the authority of a license issued by the Home Office under the Animals (Scientific Procedures) Act 1986, as amended in 2012 (and in compliance with EU Directive EU/2010/63). License applications will have been approved by the University's Ethical Review Committee (ERC) before submission to the Home Office. The ERC has a general remit to develop and oversee policy on all aspects of the use of animals on University premises and is a subcommittee of the University Court, its highest governing body.

Strains and Media. *M. tuberculosis* H37Rv was used for all experiments except p*ini*-luc and GFP release assay. The p*iniBAC*-luciferase expressing strain and a GFP-expressing *Mtb*/pMSP12 strain were used for p*ini*-luc and GFP release assays, respectively.[17] Middlebrook 7H9 (Becton Dickinson) supplemented with ADC [albumin (50 g L^{-1})/dextrose (20 g L^{-1})/NaCl (8.1 g L^{-1})], 0.2% glycerol] and 0.05% Tween 80 was used for liquid media, and Middlebrook 7H11 (Becton Dickinson) supplemented with OADC (ADC with 0.06% oleic acid) was used for solid media for in vitro growth of *Mtb*. MIC determinations were performed as previously described.[40]

The p*ini*-luc strain was grown at 1× MIC of each compound at 37 °C for 7 days in 96-well plates. Every 24 h, 50 μL of culture was taken and mixed with 50 μL of luciferase assay buffer [50 mM HEPES, pH 8.0, 0.4% Triton X100, D-luciferin (28 mg L^{-1}), 50 mM DTT]. The mixture was incubated at 37 °C for 30 min, and RLU was measured by FlUOstar Optima (BMG LABTECH). For the GFP release assay, *Mtb*/pMSP12 strain was incubated in 7H9/ADC/Tween with 30 μg/mL kanamycin in roller bottles at 37 °C to exponential phase (OD 0.2).[17] The culture was split to 30 mL in 250 mL roller bottles with test compounds added at 1× and 10× MIC and cultured for 14 days. Each day 1 mL of each culture was centrifuged at 15000*g* for 5 min. Supernatant was dispensed in 100 μL aliquots (triplicates) in consecutive wells of a 96-well black plate. GFP fluorescence was measured by FLUOstar optima (λ_{ex}485 nm and λ_{em} 520 nm) and divided by OD_{650} of the culture. For macromolecular incorporation, *Mtb* was grown to an OD_{650nm} of 0.4 in 200 mL and split into 11 mL aliquots containing test compounds. After 2 h at 37 °C, 220 μL of 0.1 mCi/ml ^{14}C-*N*-acetyl-D-glucosamine (NAG; American Radiolabeled Chemicals, Inc.) was added to each aliquot. After 24 and 48 h, 2.5 mL of NAG-labeled samples were centrifuged at 3000*g* for 10 min. The pellet was resuspended in 2 mL of $CHCl_3$/CH_3OH (2:1) and incubated at 37 °C overnight. Harvested pellets were resuspended well in 200 μL of scintillation fluid, and CPM was counted by a scintillation counter (Beckman Coulter LS6500).

Metabolomic Sample Preparation and Analysis. Samples used for metabolomic analysis of indazole sulfonamide compounds on viable *Mtb* cells were prepared using our previously published filter cultured system.[41] In short, *Mtb* was grown to mid log phase and then diluted to an OD_{600nm} of 0.1. A 1 mL culture was then inoculated onto 22 mm 0.2 μm PVDF filters (Millipore) using vacuum filtration, placed on 7H10+ADN plates, and incubated at 37 °C. On day 5 post-inoculation, *Mtb*-laden filters were transferred to plates containing DMSO vehicle, 0.5×, 1×, 5×, or 10× MIC compound **1** (or equivalent molar concentrations of its inactive congener), and incubated for 20 h, at which point there was no grossly measurable loss of viability, as previously described.[42] Samples were then metabolically quenched by plunging Mtb-laden or mock drug-exposed filters in −20 °C acetonitrile/methanol/H_2O (40:40:20). Metabolically quenched *Mtb* removed from these filters in solution was mechanically lysed with 0.1 mm silica beads in a Precellys tissue homogenizer under continuous cooling at 2 °C. Samples were then clarified by centrifugation, and the supernatant was filtered through a 0.22 μm filter. The biomass of each sample was determined by measuring residual protein content using a colorimetric assay (Pierce BCA protein assay) and used to enable intersample normalization of measured metabolite abundances. Each experiment included three technical replicates for every condition tested and was performed twice.

Samples used for metabolomic analysis of lung tissue and macrophages were prepared by mechanical lysis in −20 °C acetonitrile/methanol/H_2O (40:40:20) using a Precellys tissue homogenizer under continuous cooling at 2 °C and processed as described above. The biomass of each sample was determined by weight and used to determine lesional concentrations of guanine as described below.

Liquid Chromatography−Mass Spectrometry. Metabolites were separated using a Cogent Diamond Hydride Type C column (gradient 3) as previously described[43] and then analyzed using an Agilent 1200 liquid chromatography system coupled to an Agilent high-resolution accurate mass 6220 TOF. This system

DOI: 10.1021/acsinfecdis.6b00103
ACS Infect. Dis. 2017, 3, 18−33

achieves mass errors of approximately 5 ppm, mass resolution ranging from 10,000 to 25,000 (over m/z 121−955), and a 5 $\log_{10}$ dynamic range.

Metabolomic data sets were queried by targeted analysis using Agilent Profinder 8.0 configured to a mass tolerance of <10 ppm. Putative metabolite identities were assigned on the basis of accurate mass (m/z) and chromatographic retention time identifiers and confirmed by coelution with authentic chemical standards. Metabolite concentrations were calculated using the method of standard addition with authentic chemical standards. Metabolite abundances were normalized within experiments to residual protein biomass as described above. Absent a validated internal standard to determine absolute recovery rates, the reported metabolite abundances and concentrations likely represent underestimations. Lung tissue and macrophage guanine concentrations were determined by dividing the normalized metabolite abundances by the volume of lung tissue (assuming a lung tissue density of approximately 1 g/mL) or total cell volume of macrophages (assuming an approximate cell volume of 2.1 μL/10^6 cells[44]).

Metabolic pathway enrichment analysis was carried out using the online analytical tool MetaboAnalyst 3.0 (www.metaboanalyst.ca).[19] Enriched pathways were identified by hypergeometeric test based on a cumulative binomial distribution.

False-discovery rate (FDR)-controlling procedures are designed to control the rate of type I, or false-positive, errors in large data sets. FDR methods have greater power (sensitivity) than so-called familywise error rate (FWER) controlling methods such as Bonferroni-based corrections but provide less stringent control of type I errors.[45] The Holm−Bonferroni method[46] is a FWER controlling method used to handle the problem of multiple comparisons that is more powerful than the standard Bonferroni correction.

Generation and Characterization of Indazole Sulfonamide-Resistant Mutants. To generate mutants against the indazole sulfonamide scaffold, 50 mL of *Mtb* was grown to an OD_{650nm} of 0.2. Harvested cells were resuspended in 500 μL of medium, and 100 μL of it (10^9 cells) was plated on 7H11/OACD plates with 5×, 10×, or 50× MIC **1** and **2**. They were incubated at 37 °C for 4 weeks. After 4 weeks, the two mutants on 10× MIC compound **2** plates were inoculated in 7H9/ADC/Tween media. Genomic DNA of mutants was isolated by CTAB method.[15] Whole genome sequencing was performed and analyzed as described.[47] To confirm the large duplication of SR2.1, qPCR were performed with primer sets within the duplication region (*Rv3392*) and out of the region (*Rv3910*). These DNA fragments were amplified by 25 cycles of PCR with 0.1, 0.2, 0.4, and 1 ng of genomic DNA of SR2.1 and parental strain. The amount of amplified PCR product was compared on agarose gels. Quantitative PCR was further used to confirm amplification of guaB2 in the genome. For this, quantitative PCR was performed by real-time PCR with SYBR green. One nanogram of genomic DNA from parental strain and SR2.1 were used for each reaction. Data were normalized with 16S rRNA gene. Relative gene quantification was calculated in REST-382 version 1.[48] The intergenic sequence of wild type and mutated *guaB2* were used to replace the *hsp* promoter of pMV306hsp (Addgene plasmid no. 26155), respectively.[49] The original plasmid contains luciferase driven by the *hsp* promoter. They were electroporated into *M. smegmatis* mc^2155. Luciferase activity was measured as described above for the p*ini*-luc assay. A guanine rescue test was performed by addition of the supplements to the medium used in the MIC determination using a final concentration of 100 μM guanine, guanosine, inosine, xanthine, and hypoxanthine.

Efficacy and Validating Inhibition of Indazole Sulfonamide Scaffold against Mtb in Vitro and in Vivo. In vitro efficacy was performed in aerobic, anaerobic, and starvation conditions. For aerobic conditions logarithmically growing *Mtb* (OD_{650nm} = 0.2) was diluted 1000-fold in 1 mL of 7H9 medium and exposed to 1×, 20×, and 50× MIC of compounds **1** and **2** for up to 7 days in duplicates. After 4 and 7 days of treatment, appropriate cell dilutions were plated on 7H11/OADC plates for CFU enumeration. For anaerobic conditions, *Mtb* was cultured in the self-generated oxygen depletion model as previously described.[31] One milliliter of anaerobic *Mtb* culture was exposed for up to 3 weeks to 20× and 100× MIC compounds **1** and **2**. For the starvation condition, logarithmically growing 5 mL of *Mtb* (OD_{650nm} = 0.2) culture was washed with phosphate-buffered saline with 0.05% tyloxapol (PBST) three times and incubated in PBST for 2 weeks. Two weeks starved *Mtb* culture was aliquot to 1 mL and exposed for up to 3 weeks to compounds **1** and **2**. Dilutions were plated on 7H11/OADC plates on a weekly basis.

For the ex vivo efficacy test, J774 cells (5×10^4 cells/well) were seeded in flat-bottom 96-well plates (Corning Inc.) in DMEM GlutaMAX (Gibco) supplemented with 10% fetal bovine serum and 20 mM HEPES + 0.5 mM sodium pyruvate and infected with *Mtb* (MOI 1:1) for 24 h. Subsequently, cells were washed with PBS (pH 7.4) twice and exposed to test compounds in the above growth medium. Cells were incubated at 37 °C, 95% humidity, and 5% CO_2 for 7 days. Medium was changed after 4 days. After 7 days of incubation, 0.1% SDS was added in each well to ensure macrophage lysis. After 5 min, lysate was rapidly mixed to shear eukaryotic DNA, diluted in 7H9/ADC, and plated on 7H11/OADC plates.

For evaluation of in vivo efficacy, C57BL/6 mice were infected by the aerosol route as previously described.[50] After 14 days, groups of 10 mice were dosed with **1** and **2** given by oral gavage at 10, 30, or 100 mg/kg. Control groups were dosed with vehicle control (1% carboxymethyl cellulose) or 10 mg/kg rifampicin. After 2 and 4 weeks of treatment, groups of five mice were euthanized and appropriate dilutions in 7H9/ADC/Tween of organ homogenates plated on 7H11/OADC plates for CFU enumeration. Similarly, mice were treated by daily oral gavage with the above drugs for 2 and 4 weeks at 70 days post-infection to determine drug efficacy in chronic established infections.

To determine the length of daily exposure required to effect cidality, 3 mL of *Mtb* cell culture at OD_{650nm} of 0.2 was diluted 100-fold and exposed to test compounds as described above. Cells were exposed to compound for 3 or 6 h on a daily basis, after which test compounds were removed by centrifugation (4000*g*, 10 min) and washing with PBS three times. Washed *Mtb* cells were resuspended in 7H9/ADC/Tween without compounds and incubated at 37 °C for 21 and 18 h, respectively. Control cells were continually exposed to test compound without daily washing. This process was repeated on a daily basis for 7 days, after which appropriate dilutions were plated on 7H11/OADC plates. Similarly, to determine the daily exposure required to achieve bacteriostasis during macrophage infection, J774 cells (1×10^5 cells/well) were seeded in a 24-well plate and infected with *Mtb* at MOI 1 and exposed to test compounds as described above. Infected cells were continually exposed to compound or for daily exposure periods of 3 or 6 h followed by washing of monolayers three times with PBS and DMEM/FBS medium replacement for a total of 7 days. Cell lysis and plating were as described above.

DOI: 10.1021/acsinfecdis.6b00103
ACS Infect. Dis. 2017, 3, 18−33

To compare the level of guanine uptake of in vitro cultures of *Mtb* to *Mtb* growing inside host macrophages, ^{14}C-guanine was fed to 10^8 *Mtb* cells derived from early log-phase (OD_{650nm} = 0.2) 7H9/ADC/Tween culture or from a similar number of *Mtb* cells derived from 5-day-infected J774 cells lysed with deionized sterile water. After 3 days at 37 °C, cells were harvested by centrifugation and washed three times; a small aliquot was used for CFU enumeration by plating on 7H11/OADC agar plate, and the remaining cells were resuspended in scintillation liquid to determine guanine incorporation by scintillation counting.

Mtb IMPDH Activity and Inhibition Assays. Enzyme activity and inhibition assays were performed with recombinant truncated *Mtb* IMPDH where amino acids 126−251, corresponding to two CBS domains on the native enzyme, were substituted by two glycine residues. Truncated *Mtb* IMPDH activity was monitored by the increase in absorbance at 340 nm, due to product NADH formation ($\varepsilon_{340\ nm}$NADH = 6220 M^{-1} cm^{-1}) at 25 °C in activity buffer (Tris-HCl 50 mM, KCl 150 mM, TECEP 1.5 mM, pH 8.0). The K_M values of substrates IMP (70 ± 2 μM) and NAD (937 ± 62 μM), forward reaction k_{cat} (0.67 ± 0.01 s^{-1}), and NAD^+ substrate inhibition (10 ± 0.8 mM) of truncated *Mtb* IMPDH showed no difference when compared to native IMPDH.[12] Inhibition assays were performed on activity buffer in the presence of *Mtb* IMPDH 1 μM, IMP 0.5 mM, and NAD^+ 1 mM, in a final 50 μL volume. Compound **1**, in 100% DMSO solution, was varied from 3 nM to 800 μM. All data points, including controls, contained equal final volumes of DMSO (2 μL). All reactions were performed in triplicates. The fractional activity as a function of the inhibitor concentration was fitted to the equation $v_1/v_0 = 1/1 + ([I]/IC_{50})$ for IC_{50} value determination using SigmaPlot v.12.

K_i constants were determined by some modifications to the above protocol. Specifically, the enzymatic activity was measured by a continuous spectrophotometric assay[10] in a 200 μL reaction mixture that contained 50 mM Tris-HCl buffer, pH 8.0, 150 mM KCl, 1 mM DTT, 1 mM EDTA, 3 mM NAD^+, and 1.25 mM IMP (all chemicals were purchased from Sigma-Aldrich). After 1 min of pre-incubation, the reaction was started by adding 0.5 μg of either the *Mtb* or human enzyme and the increase in the absorbance at 340 nm, caused by the reduction of NAD^+ to NADH (ε_{340} = 6220 M^{-1} cm^{-1}), measured. The assay was performed in quartz cuvettes with a Varian Cary 50-BiO UV−visible spectrophotometer equipped with a temperature-controlled cuvette holder. The mechanism of inhibition and the K_i of compound **1** against *Mtb* GuaB2 was determined by analysis of the initial velocity data plotted against the substrate concentration (Figure 3d). The data were fitted to an equation describing the uncompetitive inhibition model using Sigma Plot-Enzyme Kinetics Module 1.3. The concentrations of compound **1** were varied from 0 to 1 μM. Data points were obtained from two independent experiments. In the case of human IMPDH, the concentration of compound **1** required to reduce the fractional enzyme activity to half of its initial value (IC_{50}) was calculated by plotting the enzyme fractional activity against the logarithm of inhibitor concentration (Figure S2) and fitting the curves to a dose−response curve (eq 2)

$$y = \min + ((\max - \min/(1 + 10^{(\log IC_{50} - x)})) \quad (2)$$

in which y is the fractional activity of the enzyme in the presence of inhibitor at concentration [I], max is the maximum value of y observed at [I] = 0, and min is the minimum limiting value of y at high inhibitor concentrations.

Chemistry. Compound syntheses and analytical data are described in the Supporting Information.

Cloning, Expression, and Protein Purification. The *M. thermoresistible GuaB2* gene was amplified from genomic DNA and cloned into the pHat2 vector without the two CBS domains and a glycine−glycine linker connecting the two parts of the catalytic region (*Mth* IMPDH ΔCBS). The *Mth* IMPDH ΔCBS protein was expressed in BL21 DE3 (NEB) cells at 37 °C until the OD_{600nm} measured 0.6, then the temperature was reduced to 18 °C, and IPTG was added at a final concentration of 500 μM. Cells were left growing overnight. Cells were harvested by centrifugation and resuspended in 50 mM Hepes, pH 8.0, 500 mM NaCl, 5% glycerol, 10 mM β-mercaptoethanol, and 20 mM imidazole. Lysis was performed using an Emulsiflex cell disruptor (Avastin). Clarification of the lysate was achieved by high-speed centrifugation and filtration through a 0.45 μm filter. The clarified supernatant was then applied to a Hi-Trap IMAC FF column (GE Healthcare) charged with nickel. The bound protein was eluted with lysis buffer + 250 mM imidazole. Overnight dialysis into lysis buffer−imidazole was performed, including incubation with TEV protease to remove the N-terminal His-Tag. Then, to remove both uncleaved protein and protease, the sample was passed through a gravity flow nickel column. The flow-through from this step was concentrated and injected onto a Superdex 200 gel filtration column pre-equilibrated with 20 mM Hepesn pH 8.0, 500 mM NaCl, 5% glycerol, and 1 mM TCEP. Elution fractions were collected and concentrated to 12.5 mg/mL for crystallization.

Chemoproteomics. The chemoproteomic affinity capturing experiments were performed as previously described.[28,29] Briefly, Sepharose beads were derivatized with **5** at 1 mM concentration, and beads were washed and equilibrated in lysis buffer [50 mM Tris-HCl, pH 7.4, 0.4% Igepal-CA630, 1.5 mM $MgCl_2$, 5% glycerol, 150 mM NaCl, 25 mM NaF, 1 mM Na_3VO_4, 1 mM DTT, and one Complete EDTA-free protease inhibitor tablet (Roche) per 25 mL]. They were incubated at 4 °C for 1 h either with 0.1 mL (0.3 mg) *M. bovis* BCG extract or with 1 mL (5 mg) mixed HEK293/K-562/placenta extract, which was pre-incubated with compound or DMSO (vehicle control). Beads were transferred either to filter plates [Durapore (PVDF membrane, Merck Millipore] or to disposable columns (MoBiTec), washed extensively with lysis buffer, and eluted with SDS sample buffer. Proteins were alkylated, separated on 4−12% Bis-Tris NuPAGE (Life Technologies), and stained with colloidal Coomassie. Gel lanes were cut into three slices and subjected to in-gel digest using LysC for 2 h and trypsin overnight.[28] Digestion, labeling with TMT isobaric mass tags, peptide fractionation, and mass spectrometric analyses were performed.[51] Proteins were quantified by isobaric mass tagging and LC-MS/MS. The proteins.fasta file for *M. bovis* BCG was downloaded (May 11, 2011) from http://genome.tbdb.org/annotation/genome/tbdb/MultiDownloads.html and supplemented with the sequences of bovine serum albumin, porcine trypsin, and mouse, rat, sheep, and dog keratins. Decoy versions of all proteins were created and added. The search database contained a total of 11,492 protein sequences, 50% forward, 50% reverse. Protein identification and quantification were performed.[52] Proteins identified with >1 unique peptide matches were considered for further data analysis. Apparent dissociation constants were determined by taking into account the protein depletion by the beads.[29] Raw data tables for the chemoproteomics experiments can be found in the Supporting Information, Tables S4−S9.

DOI: 10.1021/acsinfecdis.6b00103
ACS Infect. Dis. 2017, 3, 18−33

Crystallization, Compound Soaking, and X-ray Data Collection. The *Mth* IMPDH ΔCBS protein crystallized in 2 μL hanging drops in a 1:1 ratio with 100 mM sodium acetate, pH 5.5, 200 mM calcium chloride, and 8−14% isopropanol. Crystals appeared after 24 h and grew to full size within a week. Crystals were soaked overnight in drops of well solution + 5 mM IMP and 5 mM compound **1** dissolved in water or for 3 days in 1 mM compound **6** solubilized in 100% DMSO. Cryoprotected crystals were passed through drops containing well solution + 25% glycerol and were subsequently flash-frozen in liquid nitrogen. Data were collected from the crystals at Diamond Light Source beamline I03 (compound **1**) and I04 (compound **6**).

Structure Solution, Ligand Fitting, and Refinement. Data were processed using XDS[53] and Pointless (ccp4). To solve the structure, molecular replacement was performed with Phenix Phaser[54] using a previously solved IMP-bound *Mth* IMPDH ΔCBS structure as a probe, with the NAD site empty (unpublished data). Refinement was performed using Phenix.refine and manually in Coot.[55] IMP and compound **1** were sequentially fitted into the density using the LigandFit function of Phenix, and the structures were manually refined further using Coot. Final R/Rfree scores obtained were 0.21/0.20 for compound **1** and 0.20/0.19 for compound **6**, respectively. Information regarding the crystallographic statistics can be found in Table S10. All figures were made using Pymol (Schrodinger) and Coot. Protein−ligand interactions were analyzed using Arpeggio (H. Jubb, unpublished software).

Structures have been deposited in the protein data bank (PDB) as 5K4X for IMPDH/IMP/compound **1** and 5K4Z for IMPDH/IMP/compound **6** complex structures.

Mouse Pharmacokinetics and Bronchoalveolar Lavage (BAL) Studies. Test compound was dosed to female C57BL/6 mice (n = 3) orally by gavage as a fine suspension at 5, 30, and 100 mg/kg free base [dose volume, 10 mL/kg; dose vehicle, 1% carboxymethyl cellulose (CMC)]. Female C57BL/6 mice were chosen as these represent the sex and strain used for the in vivo tuberculosis efficacy models. Blood samples were taken from the tail vein of each mouse at predetermined time intervals post-dose, mixed with 2 volumes of distilled water, and stored frozen until analyzed using UPLC/MS-MS. Pharmacokinetic parameters were derived from the blood concentration time curve using PK Solutions software v 2.0 (Summit Research Services, Soquel, CA, USA).

For the bronchoalveolar lavage studies, mice were dosed at 100 mg/kg freebase as above. The BAL fluid was extracted following tracheostomy, where a small medial incision was made, and an Insyte IV catheter (20G, Becton Dickinson, UK) was inserted up to 1.5 cm inside the trachea and tied with a suture to avoid leakage during BAL sampling. Both lungs were flushed with a total of 1.0 mL (0.5 mL × 2) of ice-cold phosphate-buffered saline (PBS) and aspirated immediately after administration. Aspirated volumes were recorded exactly, and the samples were stored on ice until centrifugation. Blood samples were centrifuged at 3000 rpm for 5 min, whereas BAL samples were centrifuged at 1500 rpm for 5 min as well. Plasma and clean BAL were transferred into Eppendorf tubes, which were stored frozen in the upright position prior to analysis as detailed above. The epithelial lung fluid (ELF) drug concentration was determined as ELF drug concentration = BAL fluid drug concentration × (plasma urea concentration/BAL fluid urea concentration) after the method of Laohavaleeson et al.[56]

Mouse, Rabbit, and Human Granuloma Sample Analysis. For rabbit studies, specific pathogen-free, individually housed female NZW rabbits, weighing 2.2−2.6 kg, were used for aerosol infection by *M. tuberculosis* HN878, as previously described,[57] because it generates a representative range of human-like lesions in infected rabbits. Briefly, rabbits were exposed to *M. tuberculosis*-containing aerosol using a nose-only delivery system. Three hours post-infection, rabbits were euthanized, and serial dilutions of the lung homogenates were cultured on Middlebrook 7H11 agar plates to enumerate the number of bacterial colony-forming units (CFUs) implanted in the lungs. The infection was allowed to progress for 16−20 weeks, at which point the animals were euthanized to dissect uninvolved lung pieces and lesions as previously described.[58] Dissected lung tissue and lesions were weighed and categorized as uninvolved lung, cellular granuloma, caseous/necrotic granuloma, or cavity caseum. Each sample was homogenized in approximately 5 volumes of PBS and stored at −80 °C until analyzed.

Human samples were derived from lobectomies at National Masan Hospital. Immediately following surgery, the lung tissue was sterilely dissected into individual lesions and uninvolved lung tissue. Larger lesions (50−150 mg, individually weighed) were separated into caseum and lesion wall when possible. All samples for metabolite analysis were snap frozen in liquid nitrogen.

Mouse organ samples were obtained from three uninfected C57BL/6 mice and flash frozen on dry ice. J774 cell samples were obtained by washing monolayers of cells with PBS, scraping of cells, harvesting, removing PBS supernatant, and flash freezing the cell pellet on dry ice.

■ ASSOCIATED CONTENT

Supporting Information

The Supporting Information is available free of charge on the ACS Publications website at DOI: 10.1021/acsinfecdis.6b00103.

Compound syntheses and characterization, graphs showing determination of transcriptional activity of the *guaB2* promoter, data used to calculate IC_{50} value for C**1**, X-ray structure of IMPDH with C**6**, efficacy of indazole sulfonamides during infection of host cells, concentration dependence of guanine rescue during IMPDH inhibition and guanine levels on rabbit lung, mouse tissues, and J774 cells as well as data tables describing metabolomic data from treatment of *Mtb* with indazole sulfonamide scaffolds, data describing correlation between IC_{50} and whole cell activity, data from chemoproteomic profiling, data from crystallographic analyses, PK data, and guanine concentrations in mouse organs and J774 cells (PDF)

■ AUTHOR INFORMATION

Corresponding Author

*(H.I.B.) Phone: (301) 451-9438. E-mail: hboshoff@niaid.nih.gov.

Author Contributions

Y.P., K.A., and H.I.B. performed drug susceptibility determinations, electron microscopy analyses, macromolecular incorporation, and pini-luc and GFP release assays. Z.W., T.H., and K. Rhee. performed metabolomics and lung guanine analyses. V.D. and L.E.V. generated and/or provided lung tissue samples. Y.P. generated and characterized the mutants, performed macrophage and mouse efficacy, and evaluated time kill kinetics. J.S., A.B., and N.Z. performed enzyme IC_{50} determinations. M.R. and S.D. did enzyme kinetic evaluation. T.R.I. performed and analyzed the whole genome sequencing. T.L.B., A.P., and D.B.A. performed and analyzed all protein structural work. O.E., L.S., F.S., M.O.-C., L.E., and K. Read performed ADME assays.

DOI: 10.1021/acsinfecdis.6b00103
ACS Infect. Dis. 2017, 3, 18−33

H.P., M.B., and S.G.-D. performed biochemical and mass spectrometry experiments, S.G.-D. and G.D. designed experiments, analyzed data, and contributed to the manuscript. Synthetic and computational chemistry was done by S.R.J., C.J.M., L.A.T.C., T.B., A.R.C.S., S.H.D., D.M., K.I.B., P.A,T., M.H., F.Z., P.C.R., P.W., and S.R.G. analyzed data. H.I.B., Y.P., and C.E.B. analyzed the data and wrote the manuscript.

Notes

The authors declare no competing financial interest.

■ ACKNOWLEDGMENTS

This work was funded, in part, by the Intramural Research Program of NIAID and in part by grants from the Foundation for the National Institutes of Health with support from the Bill & Melinda Gates Foundation (to C.E.B. III, V.M., and P.W.), and the South African Medical Research Council (to V.M.). D.B.A. was supported by an NHMRC C. J. Martin Fellowship (APP1072476). D.B.A. and T.L.B received funding from the Newton Fund RCUK-CONFAP Grant awarded by The Medical Research Council (MRC) and Fundação de Amparo à Pesquisa do Estado de Minas Gerais (FAPEMIG) (MR/M026302/1). P.W. received joint funding from the Bill and Melinda Gates Foundation and Wellcome Trust for A Centre of Excellence for Lead Optimisation for Diseases of the Developing World. We acknowledge Beth Fischer and Vinod Nair for help with electron microscopy.

■ ABBREVIATIONS

IMPDH, inosine monophosphate dehydrogenase; *Mtb*, *Mycobacterium tuberculosis*; HGPRT, hypoxanthine−guanine phosphoribosyltransferase; IMP, inosine monophosphate; XMP, xanthosine monophosphate; MIC, minimum inhibitory concentration

■ REFERENCES

(1) Zumla, A., George, A., Sharma, V., Herbert, R. H., Baroness Masham of Ilton, Oxley, A., and Oliver, M. (2015) The WHO 2014 global tuberculosis report − further to go. *Lancet Global Health 3*, e10−e12.

(2) Dheda, K., Barry, C. E., 3rd, and Maartens, G. (2016) Tuberculosis. *Lancet 387*, 1211−1226.

(3) Horsburgh, C. R., Jr., Barry, C. E., 3rd, and Lange, C. (2015) Treatment of Tuberculosis. *N. Engl. J. Med. 373*, 2149−2160.

(4) Payne, D. J., Gwynn, M. N., Holmes, D. J., and Pompliano, D. L. (2007) Drugs for bad bugs: confronting the challenges of antibacterial discovery. *Nat. Rev. Drug Discovery 6*, 29−40.

(5) Ioerger, T. R., O'Malley, T., Liao, R., Guinn, K. M., Hickey, M. J., Mohaideen, N., Murphy, K. C., Boshoff, H. I., Mizrahi, V., Rubin, E. J., Sassetti, C. M., Barry, C. E., 3rd, Sherman, D. R., Parish, T., and Sacchettini, J. C. (2013) Identification of new drug targets and resistance mechanisms in *Mycobacterium tuberculosis*. *PLoS One 8*, e75245.

(6) Warner, D. F., Evans, J. C., and Mizrahi, V. (2014) Nucleotide Metabolism and DNA Replication. *Microbiol. Spectrum 2*, 10.1128/microbiolspec.MGM2-0001-2013

(7) Ducati, R. G., Breda, A., Basso, L. A., and Santos, D. S. (2011) Purine Salvage Pathway in *Mycobacterium tuberculosis*. *Curr. Med. Chem. 18*, 1258−1275.

(8) Long, M. C., Escuyer, V., and Parker, W. B. (2003) Identification and characterization of a unique adenosine kinase from *Mycobacterium tuberculosis*. *J. Bacteriol. 185*, 6548−6555.

(9) Meldau, R., Peter, J., Theron, G., Calligaro, G., Allwood, B., Symons, G., Khalfey, H., Ntombenhle, G., Govender, U., Binder, A., van Zyl-Smit, R., and Dheda, K. (2014) Comparison of same day diagnostic tools including Gene Xpert and unstimulated IFN-gamma for the evaluation of pleural tuberculosis: a prospective cohort study. *BMC Pulm. Med. 14*, 58.

(10) Usha, V., Gurcha, S. S., Lovering, A. L., Lloyd, A. J., Papaemmanouil, A., Reynolds, R. C., and Besra, G. S. (2011) Identification of novel diphenyl urea inhibitors of Mt-GuaB2 active against *Mycobacterium tuberculosis*. *Microbiology 157*, 290−299.

(11) Griffin, J. E., Gawronski, J. D., Dejesus, M. A., Ioerger, T. R., Akerley, B. J., and Sassetti, C. M. (2011) High-resolution phenotypic profiling defines genes essential for mycobacterial growth and cholesterol catabolism. *PLoS Pathog. 7*, e1002251.

(12) Makowska-Grzyska, M., Kim, Y., Gorla, S. K., Wei, Y., Mandapati, K., Zhang, M., Maltseva, N., Modi, G., Boshoff, H. I., Gu, M., Aldrich, C., Cuny, G. D., Hedstrom, L., and Joachimiak, A. (2015) *Mycobacterium tuberculosis* IMPDH in Complexes with Substrates, Products and Antitubercular Compounds. *PLoS One 10*, e0138976.

(13) Chen, L., Wilson, D. J., Xu, Y., Aldrich, C. C., Felczak, K., Sham, Y. Y., and Pankiewicz, K. W. (2010) Triazole-linked inhibitors of inosine monophosphate dehydrogenase from human and *Mycobacterium tuberculosis*. *J. Med. Chem. 53*, 4768−4778.

(14) Usha, V., Hobrath, J. V., Gurcha, S. S., Reynolds, R. C., and Besra, G. S. (2012) Identification of novel Mt-Guab2 inhibitor series active against *M. tuberculosis*. *PLoS One 7*, e33886.

(15) Alland, D., Steyn, A. J., Weisbrod, T., Aldrich, K., and Jacobs, W. R., Jr. (2000) Characterization of the *Mycobacterium tuberculosis* iniBAC promoter, a promoter that responds to cell wall biosynthesis inhibition. *J. Bacteriol. 182*, 1802−1811.

(16) Lee, R. E., Protopopova, M., Crooks, E., Slayden, R. A., Terrot, M., and Barry, C. E., 3rd. (2003) Combinatorial lead optimization of [1,2]-diamines based on ethambutol as potential antituberculosis preclinical candidates. *J. Comb. Chem. 5*, 172−187.

(17) Kumar, P., Arora, K., Lloyd, J. R., Lee, I. Y., Nair, V., Fischer, E., Boshoff, H. I., and Barry, C. E., 3rd. (2012) Meropenem inhibits D,D-carboxypeptidase activity in *Mycobacterium tuberculosis*. *Mol. Microbiol. 86*, 367−381.

(18) Tahlan, K., Wilson, R., Kastrinsky, D. B., Arora, K., Nair, V., Fischer, E., Barnes, S. W., Walker, J. R., Alland, D., Barry, C. E., 3rd, and Boshoff, H. I. (2012) SQ109 targets MmpL3, a membrane transporter of trehalose monomycolate involved in mycolic acid donation to the cell wall core of *Mycobacterium tuberculosis*. *Antimicrob. Agents Chemother. 56*, 1797−1809.

(19) Xia, J., Sinelnikov, I. V., Han, B., and Wishart, D. S. (2015) MetaboAnalyst 3.0 − making metabolomics more meaningful. *Nucleic Acids Res. 43*, W251−257.

(20) Pires, D. E., Chen, J., Blundell, T. L., and Ascher, D. B. (2016) In silico functional dissection of saturation mutagenesis: Interpreting the relationship between phenotypes and changes in protein stability, interactions and activity. *Sci. Rep. 6*, 19848.

(21) Worth, C. L., Preissner, R., and Blundell, T. L. (2011) SDM − a server for predicting effects of mutations on protein stability and malfunction. *Nucleic Acids Res. 39*, W215−222.

(22) Pires, D. E., Ascher, D. B., and Blundell, T. L. (2014) mCSM: predicting the effects of mutations in proteins using graph-based signatures. *Bioinformatics 30*, 335−342.

(23) Pires, D. E., Ascher, D. B., and Blundell, T. L. (2014) DUET: a server for predicting effects of mutations on protein stability using an integrated computational approach. *Nucleic Acids Res. 42*, W314−319.

(24) Pires, D. E., Blundell, T. L., and Ascher, D. B. (2015) Platinum: a database of experimentally measured effects of mutations on structurally defined protein-ligand complexes. *Nucleic Acids Res. 43*, D387−391.

(25) Hedstrom, L., Liechti, G., Goldberg, J. B., and Gollapalli, D. R. (2011) The antibiotic potential of prokaryotic IMP dehydrogenase inhibitors. *Curr. Med. Chem. 18*, 1909−1918.

(26) Biazus, G., Schneider, C. Z., Palma, M. S., Basso, L. A., and Santos, D. S. (2009) Hypoxanthine-guanine phosphoribosyltransferase from *Mycobacterium tuberculosis* H37Rv: cloning, expression, and biochemical characterization. *Protein Expression Purif. 66*, 185−190.

(27) Zhang, R., Evans, G., Rotella, F. J., Westbrook, E. M., Beno, D., Huberman, E., Joachimiak, A., and Collart, F. R. (1999) Characteristics

DOI: 10.1021/acsinfecdis.6b00103
ACS Infect. Dis. 2017, 3, 18−33

and crystal structure of bacterial inosine-5′-monophosphate dehydrogenase. *Biochemistry 38*, 4691−4700.
(28) Cox, J. A. G., Abrahams, K. A., Alemparte, C., Ghidelli-Disse, S., Rullas, J., Angulo-Barturen, I., Singh, A., Gurcha, S. S., Nataraj, V., Bethell, S., Remuiñán, M. J., Encinas, L., Jervis, P. J., Cammack, N. C., Bhatt, A., Kruse, U., Bantscheff, M., Fütterer, K., Barros, D., Ballell, L., Drewes, G., and Besra, G. S. (2016) THPP target assignment reveals EchA6 as an essential fatty acid shuttle in mycobacteria. *Nature Microbiology 1*, 15006.
(29) Bantscheff, M., Hopf, C., Savitski, M. M., Dittmann, A., Grandi, P., Michon, A. M., Schlegl, J., Abraham, Y., Becher, I., Bergamini, G., Boesche, M., Delling, M., Dumpelfeld, B., Eberhard, D., Huthmacher, C., Mathieson, T., Poeckel, D., Reader, V., Strunk, K., Sweetman, G., Kruse, U., Neubauer, G., Ramsden, N. G., and Drewes, G. (2011) Chemoproteomics profiling of HDAC inhibitors reveals selective targeting of HDAC complexes. *Nat. Biotechnol. 29*, 255−265.
(30) Gill, W. P., Harik, N. S., Whiddon, M. R., Liao, R. P., Mittler, J. E., and Sherman, D. R. (2009) A replication clock for *Mycobacterium tuberculosis*. *Nat. Med. 15*, 211−214.
(31) Boshoff, H. I., Xu, X., Tahlan, K., Dowd, C. S., Pethe, K., Camacho, L. R., Park, T. H., Yun, C. S., Schnappinger, D., Ehrt, S., Williams, K. J., and Barry, C. E., 3rd. (2008) Biosynthesis and recycling of nicotinamide cofactors in *Mycobacterium tuberculosis*. An essential role for NAD in nonreplicating bacilli. *J. Biol. Chem. 283*, 19329−19341.
(32) Via, L. E., Lin, P. L., Ray, S. M., Carrillo, J., Allen, S. S., Eum, S. Y., Taylor, K., Klein, E., Manjunatha, U., Gonzales, J., Lee, E. G., Park, S. K., Raleigh, J. A., Cho, S. N., McMurray, D. N., Flynn, J. L., and Barry, C. E., 3rd (2008) Tuberculous granulomas are hypoxic in guinea pigs, rabbits, and nonhuman primates. *Infect. Immun. 76*, 2333−2340.
(33) Simmonds, R. J., and Harkness, R. A. (1981) High-performance liquid chromatographic methods for base and nucleoside analysis in extracellular fluids and in cells. *J. Chromatogr., Biomed. Appl. 226*, 369−381.
(34) Brosch, R., Gordon, S. V., Buchrieser, C., Pym, A. S., Garnier, T., and Cole, S. T. (2000) Comparative genomics uncovers large tandem chromosomal duplications in *Mycobacterium bovis* BCG Pasteur. *Yeast 17*, 111−123.
(35) Weiner, B., Gomez, J., Victor, T. C., Warren, R. M., Sloutsky, A., Plikaytis, B. B., Posey, J. E., van Helden, P. D., Gey van Pittius, N. C., Koehrsen, M., Sisk, P., Stolte, C., White, J., Gagneux, S., Birren, B., Hung, D., Murray, M., and Galagan, J. (2012) Independent large scale duplications in multiple *M. tuberculosis* lineages overlapping the same genomic region. *PLoS One 7*, e26038.
(36) Domenech, P., Kolly, G. S., Leon-Solis, L., Fallow, A., and Reed, M. B. (2010) Massive gene duplication event among clinical isolates of the *Mycobacterium tuberculosis* W/Beijing family. *J. Bacteriol. 192*, 4562−4570.
(37) Domenech, P., Rog, A., Moolji, J. U., Radomski, N., Fallow, A., Leon-Solis, L., Bowes, J., Behr, M. A., and Reed, M. B. (2014) Origins of a 350-kilobase genomic duplication in *Mycobacterium tuberculosis* and its impact on virulence. *Infect. Immun. 82*, 2902−2912.
(38) Bennett, B. D., Kimball, E. H., Gao, M., Osterhout, R., Van Dien, S. J., and Rabinowitz, J. D. (2009) Absolute metabolite concentrations and implied enzyme active site occupancy in *Escherichia coli*. *Nat. Chem. Biol. 5*, 593−599.
(39) Park, J. O., Rubin, S. A., Xu, Y. F., Amador-Noguez, D., Fan, J., Shlomi, T., and Rabinowitz, J. D. (2016) Metabolite concentrations, fluxes and free energies imply efficient enzyme usage. *Nat. Chem. Biol. 12*, 482−489.
(40) Duckworth, B. P., Wilson, D. J., Nelson, K. M., Boshoff, H. I., Barry, C. E., 3rd, and Aldrich, C. C. (2012) Development of a selective activity-based probe for adenylating enzymes: profiling MbtA involved in siderophore biosynthesis from *Mycobacterium tuberculosis*. *ACS Chem. Biol. 7*, 1653−1658.
(41) de Carvalho, L. P., Fischer, S. M., Marrero, J., Nathan, C., Ehrt, S., and Rhee, K. Y. (2010) Metabolomics of *Mycobacterium tuberculosis* reveals compartmentalized co-catabolism of carbon substrates. *Chem. Biol. 17*, 1122−1131.
(42) Nandakumar, M., Nathan, C., and Rhee, K. Y. (2014) Isocitrate lyase mediates broad antibiotic tolerance in *Mycobacterium tuberculosis*. *Nat. Commun. 5*, 10.1038/ncomms5306
(43) Pesek, J. J., Matyska, M. T., Loo, J. A., Fischer, S. M., and Sana, T. R. (2009) Analysis of hydrophilic metabolites in physiological fluids by HPLC-MS using a silica hydride-based stationary phase. *J. Sep Sci. 32*, 2200−2208.
(44) Melmed, R. N., Karanian, P. J., and Berlin, R. D. (1981) Control of cell volume in the J774 macrophage by microtubule disassembly and cyclic AMP. *J. Cell Biol. 90*, 761−768.
(45) Benjamini, Y., and Hochberg, Y. (1995) Controlling the False Discovery Rate: A Practical and Powerful Approach to Multiple Testing. *J. R. Stat. Soc. Ser. B (Methodological) 57*, 289−300.
(46) Holm, S. (1979) A Simple Sequentially Rejective Multiple Test Procedure. *Scand. J. Stat. 6*, 65−70.
(47) Ioerger, T. R., Feng, Y., Ganesula, K., Chen, X., Dobos, K. M., Fortune, S., Jacobs, W. R., Jr., Mizrahi, V., Parish, T., Rubin, E., Sassetti, C., and Sacchettini, J. C. (2010) Variation among genome sequences of H37Rv strains of *Mycobacterium tuberculosis* from multiple laboratories. *J. Bacteriol. 192*, 3645−3653.
(48) Pfaffl, M. W., Horgan, G. W., and Dempfle, L. (2002) Relative expression software tool (REST) for group-wise comparison and statistical analysis of relative expression results in real-time PCR. *Nucleic Acids Res. 30*, e36.
(49) Andreu, N., Zelmer, A., Fletcher, T., Elkington, P. T., Ward, T. H., Ripoll, J., Parish, T., Bancroft, G. J., Schaible, U., Robertson, B. D., and Wiles, S. (2010) Optimisation of bioluminescent reporters for use with mycobacteria. *PLoS One 5*, e10777.
(50) Singh, R., Barry, C. E., 3rd, and Boshoff, H. I. (2010) The three RelE homologs of *Mycobacterium tuberculosis* have individual, drug-specific effects on bacterial antibiotic tolerance. *J. Bacteriol. 192*, 1279−1291.
(51) Savitski, M. M., Fischer, F., Mathieson, T., Sweetman, G., Lang, M. J., and Bantscheff, M. (2010) Targeted Data Acquisition for Improved Reproducibility and Robustness of Proteomic Mass Spectrometry Assays. *J. Am. Soc. Mass Spectrom. 21*, 1668−1679.
(52) Werner, T., Sweetman, G., Savitski, M. F., Mathieson, T., Bantscheff, M., and Savitski, M. M. (2014) Ion coalescence of neutron encoded TMT 10-plex reporter ions. *Anal. Chem. 86*, 3594−3601.
(53) Kabsch, W. (2010) *Acta Crystallogr., Sect. D: Biol. Crystallogr. 66*, 125−132.
(54) Adams, P. D., Afonine, P. V., Bunkoczi, G., Chen, V. B., Davis, I. W., Echols, N., Headd, J. J., Hung, L. W., Kapral, G. J., Grosse-Kunstleve, R. W., McCoy, A. J., Moriarty, N. W., Oeffner, R., Read, R. J., Richardson, D. C., Richardson, J. S., Terwilliger, T. C., and Zwart, P. H. (2010) PHENIX: a comprehensive Python-based system for macromolecular structure solution. *Acta Crystallogr., Sect. D: Biol. Crystallogr. 66*, 213−221.
(55) Emsley, P., and Cowtan, K. (2004) Coot: model-building tools for molecular graphics. *Acta Crystallogr., Sect. D: Biol. Crystallogr. 60*, 2126−2132.
(56) Laohavaleeson, S., Tessier, P. R., and Nicolau, D. P. (2008) Pharmacodynamic characterization of ceftobiprole in experimental pneumonia caused by phenotypically diverse *Staphylococcus aureus* strains. *Antimicrob. Agents Chemother. 52*, 2389−2394.
(57) Subbian, S., Tsenova, L., Yang, G., O'Brien, P., Parsons, S., Peixoto, B., Taylor, L., Fallows, D., and Kaplan, G. (2011) Chronic pulmonary cavitary tuberculosis in rabbits: a failed host immune response. *Open Biol. 1*, 110016.
(58) Prideaux, B., Via, L. E., Zimmerman, M. D., Eum, S., Sarathy, J., O'Brien, P., Chen, C., Kaya, F., Weiner, D. M., Chen, P. Y., Song, T., Lee, M., Shim, T. S., Cho, J. S., Kim, W., Cho, S. N., Olivier, K. N., Barry, C. E., 3rd, and Dartois, V. (2015) The association between sterilizing activity and drug distribution into tuberculosis lesions. *Nat. Med. 21*, 1223−1227.

DOI: 10.1021/acsinfecdis.6b00103
ACS Infect. Dis. 2017, 3, 18−33